Answer to reviewer's comments:

We thank the reviewers for their time and effort in reviewing this paper, for their thoughtful comments and suggestions, which have helped turn this into a higher-quality paper. Please find below detailed responses to the reviewers' comments.

Anonymous Referee #1

Summary This paper puts together WRF model simulations and field campaign data from the WFIP2 campaign and satellite observations to illustrate the role of moun- tain waves in stably stratified conditions on wind oscillations in wind parks and conse- quences for wind energy production and its forecasting. I find the paper addresses a relevant and relatively new topic and the authors have a unique set of data (model and observations) available to study this topic. At the same time I think the paper has to become more mature before it can be published. Overall I have the feeling the model results and observations offers much more opportunity for discussion and that there is more to be learnt from the data offered.

Thank you for your time and efforts to review this paper. We have addressed your specific comments below.

Major remarks:

1. Abstract should be rewritten. The sentence "This paper aims at understanding how mountain waves form in the complex terrain of the Columbia Basin, subsequently affect wind energy production, and impact aspects of operational forecasting, wind power plant layout, and integration of power into the electrical grid." is more like an announcement of the goal of the study, but in the abstract the reader expects concretely what has been learnt about from the study.

Thank you for this comment. We agree and have revised the abstract accordingly. The abstract now reads:

Large mountains can modify the weather downstream of the terrain. In particular, when stably stratified air ascends a mountain barrier, buoyancy perturbations develop. These perturbations can trigger mountain waves downstream of the mountains that can reach deep into the atmospheric boundary layer where wind turbines operate. Several such cases of mountain waves occurred during the Second Wind Forecast Improvement Project (WFIP2) in the Columbia Basin in the lee of the Cascade Mountains bounding the states of Washington and Oregon in the Pacific Northwest of the United States. Signals from the mountain waves appear in boundary-layer sodar and lidar observations as well as in nacelle wind speeds and power observations from wind plants. Weather Research and Forecasting model simulations also produce mountain waves and are compared to satellite observations, lidar, and sodar observations. Simulated mountain wave wavelengths and wave propagation speeds are analysed using the Fast Fourier Transform. We found that not all mountain waves exhibit the same speed and conclude that the speed of propagation, magnitudes of wind speeds, or wavelengths are important parameters for forecasters to recognize the risk for mountain waves and associated large drops or surges in power. When analysing wind farm power output and nacelle wind speeds, we found that even small oscillations in wind speed caused by mountain waves can induce oscillations between full rated power of a wind farm and half of the power output, depending on the position of the mountain wave's crests and troughs. For the wind plant analysed in this paper, 11% of the total wind farm output is influenced by the presence of mountain waves. Oscillations in measured wind speeds agree well with WRF simulations in timing and magnitude. We conclude that mountain waves can impact wind turbine and wind farm power output and, therefore, should be considered in complex terrain when designing, building, and forecasting for wind farms.

2. Title: I recommend to revise the title. The current title kind of gives the reader the expectation that a general and new theory is presented. However, the paper itself report mainly about a WRF study for a single case study for a specific region where the campaign was held. So these aspects should be included/reflected in the manuscript title. Otherwise it puts the reader on the wrong track.

Thank you for this comment. You have a point in that we only analyzed case studies in the Columbia River Basin; however, as we point out in this paper, so far mountain waves have only anecdotally been recognized to impact wind farm production, and not quantified with regards to their impact on wind energy - we could not find a single paper that discussed this anywhere in the world. Our study shows that mountain waves impact wind power generation during two events (note that another paper was submitted analyzing another three events, and the WFIP2 event log marked a high number of mountain wave cases relevant to wind energy (see new Figure 3)). While we can't prove with our study that this is true everywhere in the world, we also don't say that "all" mountain waves impact wind power generation "all the time".

In the discussion section, we link the impact of mountain waves to operational forecasting aspects, and highlight the importance of considering mountain waves when designing and building wind farms as well. Many of these aspects are applicable to many wind farms, but probably not all. Ultimately, it might also depend on the peculiarities of the power market one is operating in.

Lastly, in a way, we see this paper as a wake-up call to alert wind farm operators that they have to be careful when the possibility of mountain waves arises. We therefore chose a very short and strong title.

In light of your comment, we revised the title to "Mountain waves can impact wind power generation".

3. I have the feeling that papers was put together somewhat hastily in the sense that there are many figures, while many of those figures are not discussed in depth and only touched superficially or briefly. E.g. figure 8 is discussed on only 5 lines, figure 9 in 5 lines and figure 10 in 7 lines, Figure 11 in 4 lines, fig 12 in 8 lines, Figure 13 in 5 lines ... So overall I have the impression that not all graphs are necessary or their discussions should be deepened.

Thank you for your comment. Reviewer 2 also commented on some figures not being necessary. To address these concerns, we have rearranged (and added more discussion) the text as well as reorganized the figures. In particular, we have removed Fig. 1, moved Fig. 5 to an appendix. Fig. 7 is discussed in 10 lines, Fig. 8 is now discussed in 2 paragraphs. Fig. 9 is discussed in one paragraph (8 lines), Fig. 10 is discussed in one paragraph (8 lines), Fig. 11 in 7 lines and referenced twice more, Fig. 13 is now discussed in one paragraph (8 lines).
We do not think that the number of lines used to describe a figure is indicative of whether a figure should be in the paper or not, though we hope the additional information we provided will aid a reader in their understanding. We feel that the remaining figures in this manuscript are needed to tell the story and solidify our points.

4. The paper can be strengthened to include more information about the upscaling of the result. The authors elaborate on one case out of two they know when the mountain waves are relevant. It would be interesting whether the authors can say something about how often this occurs based on e.g. ERA5 data (so in a climatological sense) and how much forecast error is expected also in power forecast. Or how often the error is in a certain range (contingency table). This helps to put the paper in a broader perspective than the case study it is now.

Thank you for your comment. Unfortunately, ERA5 data are too coarse (roughly 30 km grid spacing at these latitudes) to resolve mountain waves. However, Figure 4 presents the distribution of mountain waves during the WFIP2 field campaign, which lasted 18 months, thus includes all the seasons. From that figure it is clear that mountain waves occurred 17% of the time during these 18 months, which gives a nice overview of how prevalent they are. We included more language discussing which of these events were deemed having a high impact on wind energy forecasting, and revised Figure 4 to include this new information also visually.

Minor remarks:

Ln 18: Large mountains: perhaps it is good to add some scale that you mean with “large”. You only mean Rockies or would the Alps or Pyrenees also be considered? Where is the cut off?

This is a good comment, however, the abstract is not a good place to cite papers that discuss this. Therefore, we left it by “large” in the abstract. In general, the scale refers to many aspects, such as the aspect ratio of the width and height of the mountain (Bauer, M. H., G. J. Mayr, I. Vergeiner, and H. Pichler, 2000: Strongly Nonlinear Flow over and around a Three-Dimensional Mountain as a Function of the Horizontal Aspect Ratio. *J. Atmos. Sci.*, **57**, 3971–3991, https://doi.org/10.1175/1520-0469(2001)058<3971:SNFOAA>2.0.CO;2.), in combination with certain conditions of the atmosphere that we have listed by citing Reichman (1978) and Mastaler and Renno (2003). For example, if the width of the mountain is too small, air may go around the mountain instead of over it. A good measure for this is the nondimensional mountain height, which is explained in Bauer et al. 2000. Their figure 13 gives a good visual explanation of this.
We have refrained from adding more information in the text as we have cited Reinecke and Durran (2007), who in turn have cited Bauer et al. 2000.

Ln 136: Mellow -> Mellor
Corrected as suggested

Ln 140: please add a few sentences why Allaerts et al was so positive about this setup that you used it here as well.

This setup has been used for many years in the Department of Energy Mesoscale-to-Microscale coupling project we have been participating in to conduct mesoscale simulations. It was constructed with input from researchers in the project based on their experience, and has been successfully used since. Allaers et al. is one example where it was used. We have updated the explanation in the paper and cited a report that better explains the project.

Ln 169: perhaps good to add the formula for the Scorer parameter, since I can image that it is not common for the complete readership you want to serve.
Good point, thanks. We have added the formula.

Figure 6: it would be helpful to have line in panel a that shows where cross sections b) and c) are taken.
Thank you for this comment. We have added the line and updated the figure caption.

Figure 6a: it would be helpful to have the terrain height in contours plotted in this panel as well.
Thank you for this comment. We have added terrain height and updated the caption.

Figure 8: could the panels b and c be merged? Simply two lines in one panel is much more easy to compare the evolution of the profile.
Yes, we agree, we changed the whole figure.

Section 3.2.2: I find that section be written much more in a quantitative way, with more information about the wavelengths involved and how much WRF overestimated the wind speed in m/s at which particular height. Also how do I see the waves in these plots? I do see alternating wind speeds at some levels, but are these waves or

This paragraph starts out with “Observations at fixed locations (such as from lidar or sodar) can reveal the presence of trapped lee waves through temporal fluctuations in the lee-wave pattern. Periods of alternating high and low wind speeds were observed at Wasco from all collocated remote sensing instruments as well as in the simulated horizontal wind field”, which explains how you can see waves in these plots, namely through alternating high and low wind speed bands. We added some text to make it clearer how to see waves in these plots: “Good agreement is found between data from all instruments (Figure 10a–c), as waves manifest in all instruments starting near 0200 UTC, increasing in amplitude until a maximum near 1000 UTC, then decreasing.” This plot is to show the signature of the waves in the observed lidar and sodar observations. In this section, we prefer to keep it qualitatively, because, as we explain in the discussion “Even though it is impossible to nail down the exact location of the wave crests and troughs, speed of propagation, magnitudes of wind speeds, or wavelength, …”, the exact timing of the waves are hard to

pinpoint. This discrepancy between model and observations should be recognized and in that sense a quantitative error analysis would be beyond the scope of this paper.

Ln 260: large: please add the scale you mean with large wavelengths.

Thank you for your comment. Large wavelengths correspond to wavelengths larger than 18 km, which is the upper limit for the band pass filtering in this work. Corresponding texts have been changed in the manuscript.

Ln 268: From the spatial pattern of mountain waves in the 100 m wind speeds: why 100 m? Is the picture consistent with the behaviour at 50 and at 200 m? Also I miss a discussion here how the model resolution may have limited the wave behaviour scale. If these are horizontally propagating waves one could also use the WRF tslist tool to include multiple receptors point on the line where the FFT was performed. The advantage of this is the higher time resolution that is obtained so one is less restricted to the model resolution.

Thank you for your comment. We choose the 100m wind speed because that is the hub-height level for most of the wind turbines in the WFIP2 region. Below you can see similar plots but from 50m and 200m above ground level. As you can see, the spatial pattern of the waves are similar to that at the 100m, except that the magnitude of the wind speed increases as height increases. We added a sentence to that effect to the text.

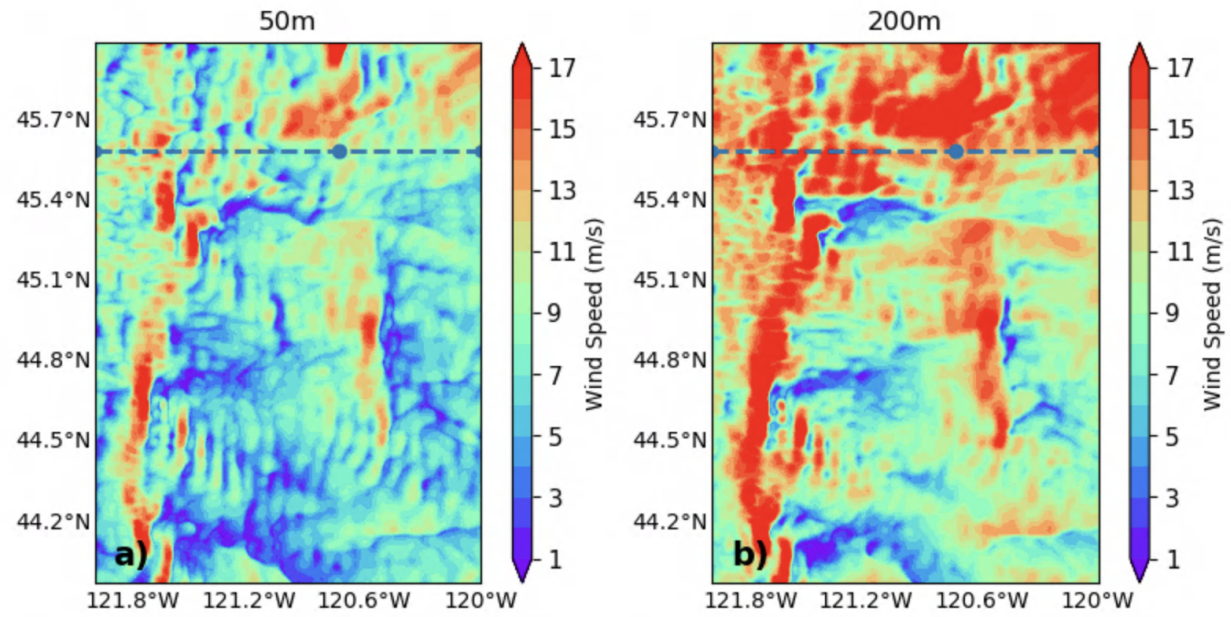

The advantage of the WRF tslist tool is to get higher temporal resolution of the wind speed. However, the power variance associated with the high frequency waves (less than 1hour) is very small. Therefore, we think that the impacts of having higher time resolution will have negligible impacts on our results.

Ln 273: “Figure 12 (a) and 12 (b) show the Hovmoller diagram of the original and recon- structed hub-height wind speed at the targeted latitude, respectively.” This sentence is technically a caption and should not be part of the main text.

Thank you for your comment. We understand your concern but we still think it is important to talk about the content of the figure before discussing it. We reworded the sentence to make it sound less like a caption.

“To confirm our choice of wavelength range, we show Hovmoller diagrams of the original and reconstructed hub-height wind speed (Figure 12) at the targeted latitude.”

Ln 283: a wave period of 1.5 h: this is inconsistent with Fig 12 c where I do not see a peak in the spectrum at 1.5 h, neither in the model nor the observations.

Thank you for your comment. Yes, you are right. It should be 2.5h, not 1.5h. Below is the revised plot which has removed the 24 hour and 12 hour spikes from both the observed and simulated wind speed (following your comments on Figure 12c). Within our period of interest (1 to 4 hour), the dominant mountain wave period is 2.5 hour.

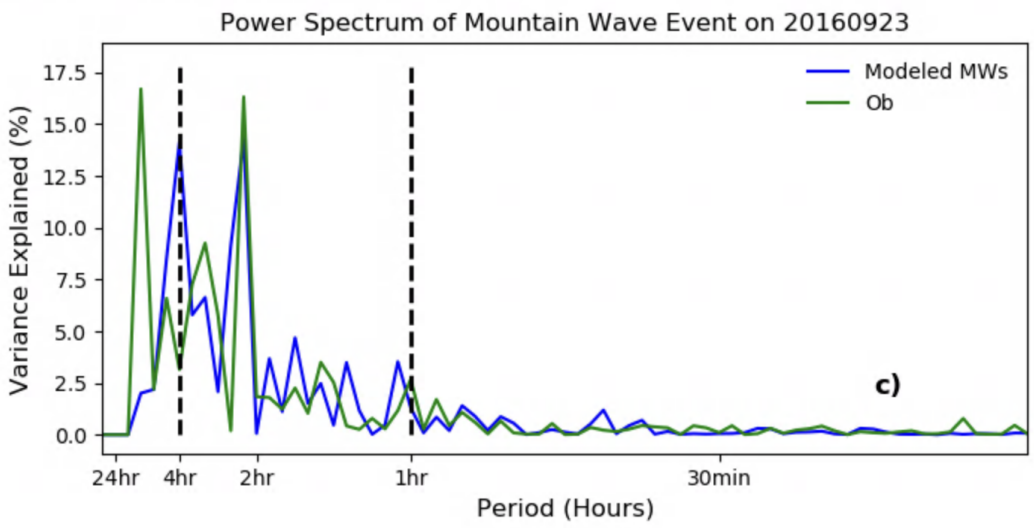

Ln 284: The results seem to be sensitive to the chosen grid point and the period of interest (not shown). This is a critical sentence that one should elaborate on. If the result is sensitive to the location, then it is also important for the forecasting. So the reader should get a better insight here how much this sensitivity is.

Thank you for your comment. Figure a) below shows the original plot from the manuscript while figure b) is a similar plot but the examined grid point is about 10 points (~7.5 km) away from that of Figure a). You can see that the corresponding pattern with the observations is stronger in Figure a) than Figure b), indicating the result is a bit sensitive to the chosen grid point. However, both patterns still match well with the observations. We have added a few more sentences to discuss this issue.

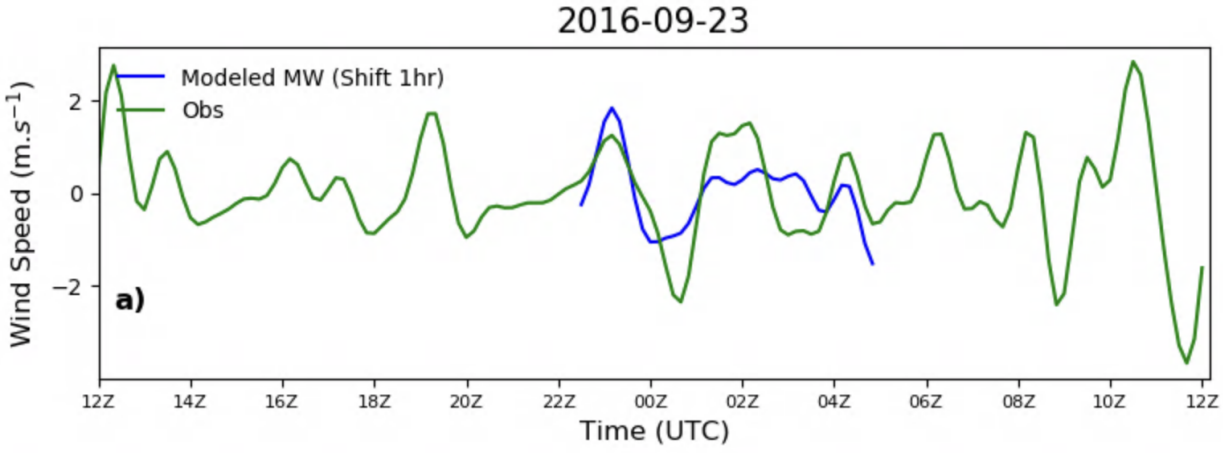

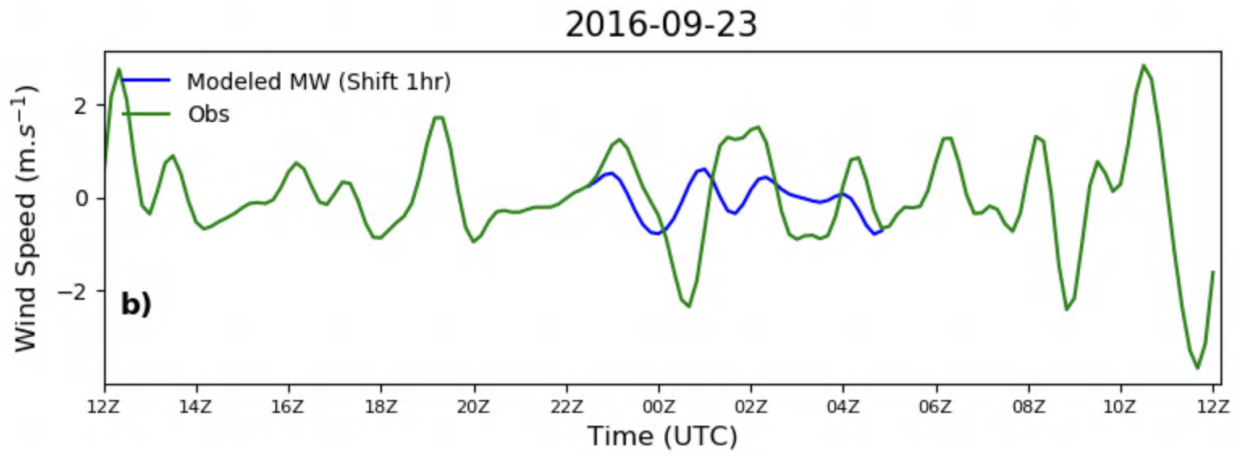

Ln 366: typo in teshold
Corrected

Figure 10: in panel b the horizontal white lines are dotted lines where in the others they are full lines.
We corrected the figure, thanks for pointing this out.

Figure 11+12: s in ms-1 should not be italic along the color bar.
Thank you for your comment. Corresponding changes have been made.

Figure 12: Panel c: please add the time period over which the spectrum was taken in the caption
Thank you for your comment. The revised plot has added dashed lines to indicate the period of interest.

Figure 12c: I am concerned with this plot, it is dominated by the energy at the diurnal cycle, (wave period of 24 h) but this is not the focus of the paper. As such the high energy peaks due to the wave are not easily identifiable. So I suggest to reshape this plot such that it better serves the aim of the paper.

Thank you for your comment. The lower frequency waves (24 hour and 12 hour) have been removed from the plot (Figure 12c) to better focus on those high energy peaks as suggested.

Figure 13b: I do not see the use of this panel. Lots of info is redundant w.r.t. to panel a. If you want to show the shifted line, then just plot it in panel a, in dashed or dotted blue line.

Thank you for your comment. We have merged those two plots into one plot as suggested.

Figure 15: The caption gives very limited information. Please add the time period or model initialization time and precise location of the three sites. Otherwise this work is not reproducible.

The data shown in Fig. 15 are proprietary data (recorded power output) from wind farm operators. They are not publicly available, nor can we disclose the exact location or time when the event occurred. We do believe that this plot is interesting, as it shows the impact of mountain waves on measured power output of 3 wind farms in the area. Unfortunately, most wind farm operators won't allow publishing details about their data, so the wind energy community has to find a way around displaying them by obscuring details.

Anonymous Referee #2

1 General comments

The paper present an interesting overview of the effect of mountain induced waves on wind farm power generation. It is an easy read and an interesting topic. I do think with some work the paper could be sharpened and for such a short paper the number of figures seems excessive. I also have some issues with the WRF model setup.

Thank you very much for your review, your time and efforts. We have addressed your comments below.

2 Specific comments

1. The WRF description lacks a lot of details and could be inadequate to model the phenomena described in the paper (difficult to judge due to missing description). For example, the ERA-interim data are used as boundary conditions, but these are at a 80 km resolution so they will lack many of scales between 80 and the 3 km that is the outer domain size of the WRF simulations used in the study. The outer domain should generally be at similar spacing of the reanalysis data used for the boundary conditions and then gradually refined using nested domains. If not, a larger buffer zone needs to be present between the reanalysis to the site of interest, but this seems not to be the case judging from Fig. 3, since winds are presumable mostly from the west. There is a larger distance between the 3 km and 750 m domain at the east side, but this is not useful because the wind is not coming from that direction. It is mentioned that there is a description in Allaerts et al., but that paper is only submitted, so as long as it is not accepted it has to be presented in this paper first. Because the paper specifically deals with waves at the scales of 10-20 km, it seems that these need to be properly resolved.

Thank you for your comment. We disagree that the outer domain should be at a similar grid spacing as the reanalysis data. This has not been followed in the literature. We have been running and designing WRF simulations for various projects without the creation of an outer nest at a similar grid spacing as the reanalysis, and even without the need of an intermediary domain. Also, in the literature you can find examples where coarse boundary conditions were downscaled without the need of an intermediary domain. As an example, Liu et al. (Liu, C., Ikeda, K., Rasmussen, R. et al. Continental-scale convection-permitting modeling of the current and future climate of North America. Clim Dyn 49, 71–95 (2017). https://doi.org/10.1007/s00382-016-3327-9) used ERA-Interim boundary conditions to run WRF on a 4-km domain. They state explicitly: “Tests showed that one-way nesting WRF, at 4-km grid spacing, with the ~75 km reanalysis was an adequate configuration without the need for a coarse grid that intermediates the ERA-Interim data and the WRF domain.”
The buffer of our domain setup consists of 40/51 grid cells on the western and southern side, which is 8-10 times more than the usually recommended buffer zone of 5 grid points. The larger distance on the eastern and northern side is due to this setup being used for many studies over the WFIP2 domain. The relation between the size of inflow and outflow boundaries is not important, as long as the buffer zone from the incoming wind direction is large enough, which is the case for this study because we used 40 and 51 grid points.
In the section Code/Data Availability, we state that the namelist is available upon request. For your convenience, we pasted the relevant sections of the WRF namelist at the end of this document.

*We are also happy to announce that the paper by Allaerts et al. is now published (*http://link.springer.com/article/10.1007/s10546-020-00538-5*). However, in light of a comment of reviewer 1 we changed the reference in the paper.*

2. Many of the plots are not really needed: for example, figure 7 and 8 are only discussed in a couple of lines. The message of these plots could easily be replaced by a few lines of text.
   Reviewer 1 had a similar comment regarding too many figures. We removed Fig. 1 and moved Fig. 5 to the appendix. We added more details to the text so that Fig. 7 is discussed in 9 + 1 lines, Fig. 8 in 2 paragraphs. We have changed Fig. 8. Replacing these figures with only text would not be sufficient in our opinion as we believe they help solidify our points to the reader.

Technical corrections

l60: There is no Wells et al. in the references
Thanks for finding this. We have added it now.

l71: Remove space before point
Corrected as suggested

108: Was there any filtering with respect to CNR threshold or other quality con- trol?

Basic quality control, requiring that an individual line-of-sight (LOS) velocity be measured with a carrier-to-noise ratio greater than -22 dB, has been applied to these data. The two-minute averages are based only on the 1-Hz LOS with CNR exceeding -22 dB. Lidars require a sufficient number of scatterers for a return signal, so clean air conditions have lower availability (Aitken et al. 2012). We have added this information to the text.

Aitken, M., L., M. E. Rhodes, and **J. K. Lundquist**. 2012. Performance of a wind-profiling lidar in the region of wind turbine rotor disks. Journal of Atmospheric and Oceanic Technology 29, 347-355.

115: Please add reference for filtering/setup of the sodar.
Thank you for this comment. We have added references for the sodar data.

l210: Brunt-Vaisala -> Brunt-Väisälä
Corrected

l132: What is temporal resolution of GOES-14?
Good point, this should be mentioned in the paper. We added it (it's every 30 min).

l136: Mellow->Mellor + add reference to the PBL scheme (Nakanishi et al.).
Corrected as suggested

l139: Isn't it usual to switch of the cumulus schemes already at those resolutions?

We believe one should have a Cumulus scheme on at dx = 3km because we are not adequately resolving many of the convective updrafts responsible for deep convection. This is why, for example, the HRRR does poorly for weakly forced air-mass thunderstorms while only getting the larger modes well (i.e., MCSs). All "mid-sized" convection in the HRRR is usually aliased up to larger scales, so it can be handled reasonably, but the scales of the updrafts are often wrong. Note that the HRRR is based on the WRF code.

Mohan and Bhati et al., (2011) analyzed the WRF model performance with parameterized cumulus in a domain over the subtropical region of Delhi, India, with a horizontal grid spacing of 2 km. They found that a combination of physical options using the Kain-Fritsch cumulus parameterization showed the best model performance during the verified period. They also found that the microphysics and cumulus parameterizations had less impact than the other physical options on the model output.

With regards to the simulated mountain wave case here, no convective precipitation is produced, so the scheme is not active. So it is practically turned off and the sentence about the cumulus scheme is not relevant. We have removed this sentence.

M. Mohan and S. Bhati, "Analysis of WRF model performance over subtropical region of Delhi, India," *Advances in Meteorology*, vol. 2011, Article ID 621235, 13 pages, 2011.

l144: Was there any grid or spectral nudging performed? I think it is a good practice anyway to include the WRF namelist, because then people can easily reproduce the results.
No, we didn't perform any nudging. As mentioned in the section about Code/Data availability, the namelist is available upon request. The relevant sections of the namelist are copied to the end of this document for your convenience.

l156: What was their criteria for defining topographic wakes?
Each week, program scientists discussed the previous 7 days, analyzing the real-time 13-km RAP, the 3-km HRRR

and 750-m HRRR-nest, global model forecasts, satellite imagery, soundings, surface observations, and wind power generation. The criteria for topographic wakes in this instance were mostly based on the available model simulations and observations: time-height plots of wind speed observations, comparison of observations in waked areas versus non-waked ones, their appearance in satellite images and the horizontal slices of simulated wind speeds (lulls). We added this information to the text.

l180: left) -> (Fig. 6, left)?
Corrected to Fig. 6 (a)

l205: Fig 6. panel c: I think this would be easier to see when you plot vertical motions as red (positive) and blue (negative). Now it seems like there is only positive motions and it is not easy to distinguish wave patterns.
Thank you for this comment. Very good point. We have adjusted the figure.

l281: It is not clear to me how the reconstruction is done. Please clarify.

Thank you for your comment. The details about the reconstruction are documented in another paper which we recently submitted to Renewable Energy (Xia et al., 2020). We have cited this work in this revision and included more details in the text.

Reference:
Xia G., Draxl C., Raghavendra A., Lundquist J.K (2020) **Validating Simulated Mountain Wave Impacts on Hub-Height Wind Speed Using SoDAR Observations,** *Submitted to Renewable Energy.*

Fig 11b: units missing for colorbar.
We added the units for the colorbar, thanks for pointing this out.

l303: Hovmoller -> Hövmöller (occurs in more places)
corrected

l326: approximately10 -> approximately 10
Corrected as suggested.

l340: Wake effects play a role at all farms, I assume. Please explain this in more detail.
Thank you for this comment. We should have been clearer here. We were talking about mountain wakes, which is now changed in the text. The exact cause of the irregularity of the other farms' oscillations would have to be looked at in more detail to draw better conclusions. However, this plot shows oscillations very nicely. As mentioned in the paper, distinguishing the effects of mountain waves, mountain wakes, and oscillations due to the meandering of the wakes is very difficult. At least for the farm discussed in detail in this paper, mountain wake effects do not play a role during the analysis time.

WRF namelist:

```
&domains
 time_step          =  10,
 max_dom            =   2,
 s_we               =   1, 1,
 e_we               = 381, 1001,
 s_sn               =   1, 1,
 e_sn               = 351, 901,
 s_vert             =   1,  1,  1, 1, 1,
 e_vert             =  88, 88, 88, 88, 88
 eta_levels         =  1.00000,  0.99935,  0.99871,  0.99806,
                       0.99742,  0.99677,  0.99609,  0.99538,
                       0.99464,  0.99386,  0.99304,  0.99218,
                       0.99127,  0.99032,  0.98933,  0.98829,
```

```
                    0.98719,  0.98605,  0.98484,  0.98358,
                    0.98226,  0.98087,  0.97941,  0.97789,
                    0.97629,  0.97461,  0.97285,  0.97101,
                    0.96908,  0.96705,  0.96493,  0.96271,
                    0.96038,  0.95793,  0.95538,  0.95270,
                    0.94989,  0.94696,  0.94388,  0.94066,
                    0.93729,  0.93360,  0.92955,  0.92512,
                    0.92026,  0.91495,  0.90914,  0.90278,
                    0.89584,  0.88825,  0.87997,  0.87095,
                    0.86112,  0.85042,  0.83879,  0.82617,
                    0.81247,  0.79764,  0.78161,  0.76430,
                    0.74566,  0.72562,  0.70412,  0.68112,
                    0.65658,  0.63048,  0.60281,  0.57359,
                    0.54285,  0.51066,  0.47711,  0.44234,
                    0.40652,  0.36985,  0.33259,  0.29501,
                    0.25746,  0.22028,  0.18491,  0.15347,
                    0.12553,  0.10069,  0.07861,  0.05898,
                    0.04154,  0.02603,  0.01225,  0.00000,
 p_top_requested         = 10000,
 num_metgrid_levels      = 38,
 num_metgrid_soil_levels  = 4,
 dx                  = 3000, 750,
 dy                  = 3000, 750,
 grid_id               =   1,  2,
 parent_id             =   1,  1,
 i_parent_start        =   1,  51,
 j_parent_start        =   1,  40,
 parent_grid_ratio     =   1,  4,
 parent_time_step_ratio  =   1,  4,
 feedback              =   0,
 smooth_option         =   0,
 /
&physics
 mp_physics            = 10, 10,
 ra_lw_physics         =  4,  4,
 ra_sw_physics         =  4,  4,
 radt                = 20, 5,
 sf_sfclay_physics     =  5,  5,
 sf_surface_physics    =  2,  2,
 bl_pbl_physics        =  5,  5,
 bldt                =  0,  0,
 cu_physics            =  1,  0,
 cudt                =  5,  0,
 isfflx              =  1,
 ifsnow                =  0,
 icloud                =  0,
 surface_input_source    =  1,
 num_soil_layers       =  4,
 sf_urban_physics      =  0,  0,
 num_land_cat          = 24,
/
&dynamics
 w_damping             =   1,
 diff_opt              =   1,   1,
 km_opt                =   4,   4,
 diff_6th_opt          =   2,   2,
 diff_6th_factor       = 0.12,0.12,
 base_temp             = 290.
 damp_opt              = 3,
 zdamp                 = 5000.,5000.,
```

```
 dampcoef              =   0.2,  0.2,
 khdif                 =    0,   0,
 kvdif                 =    0,   0,
 non_hydrostatic       = .true.,.true.,
 moist_adv_opt         =     1,    1,
 scalar_adv_opt        =     1,    1,
 tke_adv_opt           =     1,    1,
 h_mom_adv_order       =     5,    5,
 v_mom_adv_order       =     3,    3,
 h_sca_adv_order       =     5,    5,
 v_sca_adv_order       =     3,    3,
 /
&bdy_control
 spec_bdy_width        = 5,
 spec_zone             = 1,
 relax_zone            = 4,
 specified             = .true.,.false.,
 nested                = .false., .true.,
/
```

Mountain waves can impact wind power generation

Caroline Draxl[1], Rochelle P. Worsnop[2,5], Geng Xia[1], Yelena Pichugina[2,5], Duli Chand[3], Julie K. Lundquist[1,4], Justin Sharp[6], Garrett Wedam[7,8], James M. Wilczak[5], Larry K. Berg[3]

[1]National Renewable Energy Laboratory, Golden, CO 80401 USA
[2]Cooperative Institute for Research in the Environmental Sciences, University of Colorado Boulder, Boulder, CO 80309 USA
[3]Pacific Northwest National Laboratory, Richland, WA 99352 USA
[4]Department of Atmospheric and Oceanic Sciences, University of Colorado Boulder, Boulder, CO 80302 USA
[5]National Oceanic and Atmospheric Administration/Earth System Research Laboratory, Boulder, CO 80305 USA
[6]Sharply Focused, LLC, Portland, OR 97232 USA
[7]Avangrid Renewables, Portland, OR 97209 USA
[8]Natural Power, Seattle, 98121, USA

Correspondence to: Caroline Draxl (caroline.draxl@nrel.gov)

Abstract. Large mountains can modify the weather downstream of the terrain. In particular, when stably stratified air ascends a mountain barrier, buoyancy perturbations develop. These perturbations can trigger mountain waves downstream of the mountains that can reach deep into the atmospheric boundary layer where wind turbines operate. Several such cases of mountain waves occurred during the Second Wind Forecast Improvement Project (WFIP2) in the Columbia Basin in the lee of the Cascade Mountains bounding the states of Washington and Oregon in the Pacific Northwest of the United States. Signals from the mountain waves appear in boundary-layer sodar and lidar observations as well as in nacelle wind speeds and power observations from wind plants. Weather Research and Forecasting model simulations also produce mountain waves and are compared to satellite observations, lidar, and sodar observations. Simulated mountain wave wavelengths and wave propagation speeds are analysed using the Fast Fourier Transform. We found that not all mountain waves exhibit the same speed and conclude that the speed of propagation, magnitudes of wind speeds, or wavelengths are important parameters for forecasters to recognize the risk for mountain waves and associated large drops or surges in power. When analysing wind farm power output and nacelle wind speeds, we found that even small oscillations in wind speed caused by mountain waves can induce oscillations between full rated power of a wind farm and half of the power output, depending on the position of the mountain wave's crests and troughs. For the wind plant analysed in this paper, mountain wave induced fluctuations translate to approximately 11% of the total wind farm output being influenced by mountain waves. Oscillations in measured wind speeds agree well with WRF simulations in timing and magnitude. We conclude that mountain waves can impact wind turbine and

wind farm power output and, therefore, should be considered in complex terrain when designing, building, and forecasting for wind farms.

1 Introduction

As wind farm deployment in the United States and worldwide continues to increase, contributions from renewable wind energy production to the electrical-generation portfolio are also increasing (AWEA Data Services 2017; Global Wind Energy Council 2018). The U.S. Department of Energy's (DOE's) Wind Vision study (DOE 2015) mapped out a target scenario for wind energy to provide 35% of the United States' electricity demands by 2050. Wind plants are already deployed in areas of complex terrain, and will continue so, to satisfy that portfolio. Complex terrain, herein defined as terrain with irregular topography (e.g., mountains, valleys, coastlines, and canyons), can modify the flow within and far downstream of the terrain.

One area of complex terrain where numerous wind farms are deployed is the Columbia River basin in the Northwest United States, which is located east of the Cascade Range. The Cascade Range extends from southern British Columbia through Washington and Oregon to Northern California, for 1,100 km (Wikipedia), with a width of 130 km. Volcanic summits in the area reach up to approximately 4,000 m above mean sea level. During westerly flow, the Cascade Range poses an obstacle that impacts the weather and modifies the wind flow to the east of the Cascade Range, which impacts wind farm production of the deployed wind power plants in the area (Figure 1).

During westerly winds with stable atmospheric conditions, air ascends the Cascade Mountains and strong buoyancy perturbations can develop in the form of mountain waves, or lee waves, downstream of the Cascade Range. The area is prone to these conditions primarily during the cold and transition seasons, mostly during spring. Mountain waves may be nearly stationary, vertically propagating, or trapped. Vertically propagating waves are relevant to wind energy to the extent that they can lead to downslope windstorms. Trapped lee waves are relevant to wind energy because they occur in the lowest 1–5 km of the troposphere (AMS glossary, Durran 1990). With their horizontal wavelengths between 5 km and 35 km, trapped lee waves have anecdotally been recognized to impact wind farm production in the area, particularly if stationary.

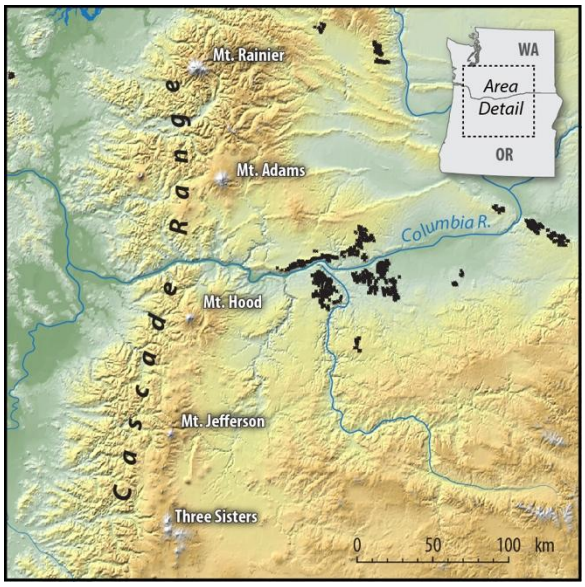

Figure 1. Map with the location of the major volcanoes (white labels) and wind farms (black dots) in the area. Figure by Billy Roberts, NREL.

The mountains of the Cascade Range can also block atmospheric flow and create a wake behind them. Mountain wakes are usually accompanied by significant drag and deceleration of low-level flow (Wells et al., 2008). During westerly winds, such mountain wakes are relevant for wind energy in the Columbia River Basin as they create meandering bands of low wind speeds that can extend hundreds of kilometres downwind and decrease power output from wind farms. Their exact timing and location are hard to predict as they meander.

Mountain waves and wakes can and commonly do occur concurrently within the Columbia River basin (Wilczak et al. 2019, Pichugina et al. 2020). In this region, mountain wakes mostly occur downstream from Mt. Hood and Mt. Adams (Figure 1), as seen from satellite observations and model simulations (examples are shown in Figure 4 and Figure 7). Both mountain waves and wakes impact wind plants and their power output. Because these phenomena can occur simultaneously and under the same conditions, distinguishing their relative impacts can be challenging. Taking advantage of the rich data set of the Second Wind Forecast Improvement Project (WFIP2; Shaw et al. 2019 and Wilczak et al. 2019) and mesoscale simulations from the Weather Research and Forecasting (WRF) model, this paper focuses on one phenomenon only—the impact of mountain waves on wind farms. Many studies have analysed mountain wakes for the last decades (e.g., Lindsay 1962; Bourgeault et al. 1993; Klemp and Lilly 1997; Doyle and Durran 2002; Durran 2003; Smith 2003; Smith and Broad 2003; Grubišić and Billings 2007; Smith et al. 2007; Mahalov et al. 2011; Nappo 2012; Vosper et al. 2012; Miglietta et al. 2013; Durran 2015; and Fritts 2015). However, even though one article (Rasheed et al. 2014) mentions that mountain waves result in horizontal and vertical wind shear, which can significantly impact wind power production, none quantified that impact. Therefore, it is our goal to document for the wind energy community, in particular for forecasters and the wind energy industry, the importance of considering mountain waves in operations and wind plant deployment. A second goal of this paper is to

what degree the mesoscale WRF model is able to capture mountain wave characteristics in the complex terrain of the Columbia Basin, a key region for wind energy production.

This paper is structured as follows: In the next section, we describe the measurements and model simulations used. We then identify and quantify mountain waves in Section 3 from a meteorological perspective and as simulated by WRF, before we analyse the impact of mountain waves on wind farm output using nacelle winds and supervisory control and data acquisition (SCADA) data. In Section 4, we provide a discussion relating our findings to practical aspects of mountain waves in forecasting and operations then conclude in Section 5 with recommendations for actions during mountain wave events.

2 Data and Methods

Our analysis is based on the extensive measurement network from the WFIP2 (Shaw et al. 2019 and Wilczak et al. 2019). WFIP2 is a DOE and National Oceanic and Atmospheric Administration (NOAA)-funded program aimed at improving the accuracy of numerical weather prediction (NWP) model forecasts of wind speed in complex terrain for wind energy applications (Wilczak et al. 2019; Banta et al. 2019; Bianco et al. 2019; Olson et al. 2019; Pichugina et al. 2019, 2020). Measurements were collected during an 18-month field campaign between October 2015 and March 2017 in the Columbia River Gorge and the Columbia Basin (Figure 1). For this paper, measurements from remote sensing instruments are used (Section 2.1) to identify mountain waves through time-series analysis, spectra, and statistics. Satellite images (Section 2.2) further help identify mountain waves, and WRF model simulations (Section 2.3) support our analysis. Nacelle wind speeds and power output from a wind farm in the area portray the influence of mountain waves on wind plants.

2.1 WFIP2 observations

To analyse wind flow variability during mountain wave events, we use profile measurements from lidars and sodars (Sections 2.1.1 and 2.1.2) that were deployed in the WFIP2 research area. These instruments continuously operated during the 18-month experiment providing real-time data. These quality-controlled data are openly available to the public through the Data Archive and Portal (DAP; https://a2e.energy.gov/data). Proprietary nacelle wind speeds from a wind farm in the area, as well as its power output (Sections 2.1.3), quantify the impact of mountain waves on wind farms.

2.1.1 Lidar data

Several profiling and scanning lidars were deployed as part of the WFIP2 field campaign. This study uses measurements from the scanning Doppler lidar and the wind profiling lidar at the Wasco site (Figure 2). The WindCube profiling lidars sample line-of-sight velocities sequentially in four cardinal directions along a nominally 28° azimuth from vertical and a nominal temporal resolution of 1 Hz (Aitken et al. 2012; Rhodes and Lundquist, 2013), simultaneously sampling ten range gates centered on 40, 60, 80, 100, 120, 140, 160, 180, 200, and 220 m AGL. These lidars provide estimates of wind speed, wind

direction, and vertical velocity within the surface layer and boundary layer up to 250 m AGL (Bodini et al, 2019) that were also used for the selection of mountain wave cases. Basic quality control, requiring that an individual line-of-sight (LOS) velocity be measured with a carrier-to-noise ratio greater than -22 dB, has been applied to these data. The two-minute averages are based only on the 1-Hz LOS with CNR exceeding -22 dB. Lidars require a sufficient number of scatterers for a return signal, so clean air conditions have lower availability (Aitken et al. 2012).

2.1.2 Sodar data

In this paper we use sodar measurements from the Wasco and Van Gilder Road sites. At Wasco, the ART VT-1 sodar model was deployed, which is a monostatic phased-array Doppler sonic detection and ranging (sodar) system. It provides a "virtual tower" for obtaining remote measurements of the wind profile up to a height of approximately 300 m at a vertical resolution of 10 m. The system includes a 48-element acoustical array. At Van Gilder Road, which is close to Wasco, a triton wind profiler is used. This profiler measures wind speed, direction, and turbulence intensity at heights from 30 m to 200 m above ground every 10 min. The quality-controlled sodar data are stored on the DAP. Information about setup and filtering for the Wasco and Van Gilder Road sodars can be found in Atmosphere to Electrons, 2020 (a) and Atmosphere to Electrons, 2020 (b), respectively.

2.1.3 Nacelle winds and turbine power output

We use data from approximately 100 wind turbines from a wind farm in the WFIP2 region to assess how mountain waves influence observed wind speed and power output. The wind farm is located north of the Columbia River Gorge and experienced mountain wave events during the WFIP2 field campaign. From the turbine nacelles, we use 80 m, 10 min averaged wind speed data and 10 min averaged power output. Data from a single turbine, as well as spatially aggregated winds across an entire wind plant, are compared with outputs from corresponding WRF simulations (see Section 3.2).

2.2 Satellite images

The mountain waves are detected using visible clouds features from the satellite observations. We utilized both polar orbiting and geostationary satellite observations to locate the mountain waves downwind of mountain peaks. The cloud features are retrieved from the Geostationary Operational Environmental Satellite (GOES-14) routine observation over the continental United States. To have the best cloud contrast and spatial separation, we used 1 km resolution pixels from band 1 (approximately 630 nm) of the GOES-14 satellite. The GOES retrieved mountain wave features in the form of clouds are compared with Moderate Resolution Imaging Spectroradiometer (MODIS) satellite observations for better understanding. The comparison in both satellites looks reasonable, though the MODIS observations show finer cloud features due to higher spatial resolution (0.25 km). Since MODIS observations have higher spatial resolution but limited temporal resolution (only one

MODIS satellite per day passes over the Columbia Basin), considering the temporal evaluation of waves, we decided to use the GOES-14 observations at a temporal resolution of 30 min.

2.3 WRF simulations

Model simulations at 5 min resolution produced with the WRF model version 3.7.1 augment the observational analysis. We use model output from an inner domain with a 750 m grid spacing, that was nested within a larger domain at 3 km grid spacing (Figure 2). ERA-Interim reanalysis data (Dee et al. 2011) provide initial and boundary conditions. We used the Mellor-Yamada Nakanishi and Niino Level 2.5 boundary layer and surface layer schemes (Nakanishi and Niino 2009), the Morrison double-moment microphysics scheme, the Rapid Radiative Transfer Model for Global Circulation Models, simple diffusion, and vertical velocity damping (Skamarock et al. 2008). This model setup has been successfully used in DOE's Mesoscale-to-Microscale Coupling project and was constructed with input from modeling experts in the project (e.g., Haupt et al. 2017). Computations were carried out using 88 vertical levels, up to 10,000 hPa, which were spaced approximately 5 m apart in the lowest 20 m, with the grid spacing increasing continuously beyond that. Within the turbine rotor layer (approximately 20–150 m above ground level (AGL)) the vertical resolution was 8–10 m.

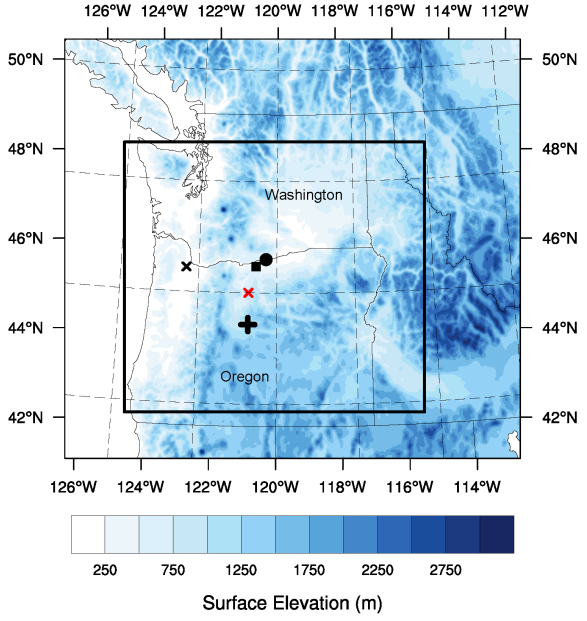

Figure 2. WRF modelling domains. The rectangle denotes the area of the 750 m domain. U.S. state boundaries are indicated. The black x denotes the location of Troutdale, the cross Prineville, the square Wasco and Van Gilder Road, the circle the location of the wind farm in the area, and the red x the location in the WRF domain where profiles are plotted in Figure 5. The Columbia River cuts through the Cascade Range at the border between the state of Oregon to the south and Washington to the north.

3 Results

Each week throughout the WFIP2 field program, scientists and wind energy forecasters reviewed the daily weather in the region and wrote a brief synopsis in an event log (Wilzcak et al. 2019), assessing the significance of the key phenomena (Pichugina et al. 2020) that impacted wind power generation. Key phenomena were categorized by having a "High", "Medium", and "Low" importance (%) for wind energy (WE), which was estimated by analysing all available observations, Bonneville Power Administration (BPA) power generation and schedule error, power ramps, and the performance of the NOAA's High-Resolution Rapid Refresh model (Figure 3a). From this event log, we found 95 days during the 18 months (548 days) where mountain wave activity was indicated by a meteorologist, so that mountain waves were present at least 17% of the time. Each of the key phenomena were categorized further by three levels of significance (Potential, Interesting/Relevant, or Not currently of interest). The significance of mountain wave cases for each level of importance relative to all phenomena is shown in Figure 3a.

As noted in the introduction, topographic wakes often occur simultaneously with mountain waves. During WFIP2, topographic wakes were recorded in the event log 15% of the time, based on analysis of wind speed observations, comparisons of observations in waked versus nonwaked areas, and their appearance in satellite images and horizontal slices of simulated wind speeds. Distributions of mountain waves and topographic wakes (Figure 3b) show a high frequency of both events during spring months.

Scanning this event log as well as lidar and sodar observations, we identified 2 days where mountain waves had a strong presence over the area and impacted wind farms in the Columbia Basin. The first day (11 November 2016) is documented in Wilczak et al. (2019). In this paper, we focus on the second day (24 September 2016) because of the availability of measurements and SCADA data and the presence of typical characteristics of mountain waves.

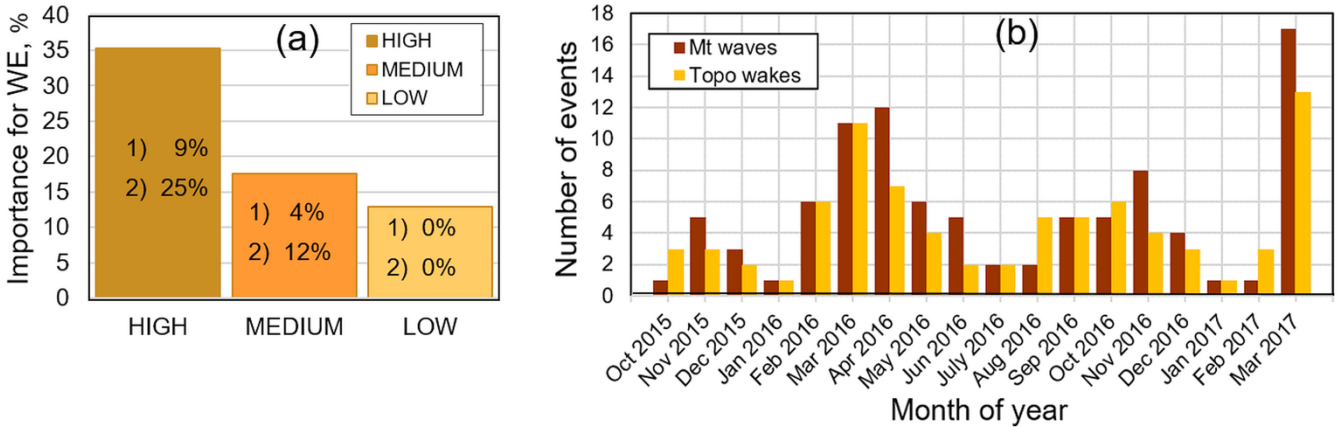

Figure 3: (a) Distribution of days during WFIP2 that exhibited observed phenomena that were ranked as of HIGH, MEDIUM, and LOW importance to wind energy according to the Event Log. The frequency of cases per level of importance that are considered a potential (1) or interesting/relevant (2) case for wind energy is given in each bar. (b) Distribution of mountain waves and topographic wakes observed during WFIP2 according to the Event Log.

3.1 Analysis of model simulations on 24 September 2016

Reichmann (1978) and Mastaler and Renno (2003) state that the best conditions for mountain waves are: (i) the presence of a stable air mass, (ii) wind speeds aloft must be greater than about 8 m s^{-1} at ridge level, (iii) the wind direction should be nearly constant throughout the stable layer, (iv) the wind speed should be constant or increasing with altitude, and (v) the wind direction should be within 30 degrees of normal to the perturbing ridge. From these conditions it is deduced that the Scorer parameter (Scorer 1949), an indicator for mountain wave development, should decrease with altitude. On 24 September 2016, all the above conditions were met in the model simulations, as will be discussed in this section.

On 24 September 2016, stationary mountain waves east of the Cascade Mountains were caused by flow from north-westerly directions. That flow, in turn, was forced by a low-pressure system over the western half of the continental United States (see Appendix). The area of the Columbia Basin was covered by clouds at 00:00 UTC, which completely dissolved by 07:30 UTC (not shown).

Mountain waves can be seen in the simulated horizontal wind field at 100 m AGL (Figure 4 (a)) as relatively thin and similarly spaced oscillating strips of high and low wind speeds oriented approximately perpendicular to the wind direction. They are triggered by the flow over the Cascade Mountains already around 23 September 2016, 16:00 UTC, and between 20:00 and 22:00 UTC they take over the whole area, impacting Prineville and a wind farm in the WFIP2 region. An elongated wake extending downstream from Mt. Hood (large triangle in Figure 4 (a)) is narrowed to a meandering band when the wakes cover the area. Wakes are also discernible downstream from Mt. Jefferson, Sisters, and Broken Top.

A cross section of the simulated horizontal wind field, potential temperature, and the PBL top from west to east on 24 September 2016, at 04:00 UTC, centered over a wind farm (Figure 4 (b)), further shows the appearance of mountain waves in the simulations, up to approximately 4.5 km above sea level, as do oscillating patterns in the vertical wind speeds (Figure 4 (c)).

The stratification of the atmosphere during the occurrence of mountain waves is shown for Troutdale, a location west (and therefore upstream) of the Cascade Mountains, and for a location in the centre of the area where waves occur (Figure 2 and Figure 5). The atmosphere is stably stratified, except from 00:00–03:00 UTC where a well-mixed layer exists below the approximately 1500 m crest height up to approximately 1 km. The simulated wind speed profiles show winds between approximately 6 m s^{-1} and 10 m s^{-1} up to approximately 2.5 km, decreasing, with a high wind shear, above 2 km. In the centre of the domain, during the time where mountain waves are present, the wind speeds are higher than at Troutdale but exhibit a similar wind shear above approximately 3 km. The stable stratification, wind speed magnitudes (satisfying the constraint from Mastaler and Renno (2003) that wind speeds aloft must be greater than about 8 m s^{-1} at ridge level), constant wind speeds below 2 km, and increased wind speeds above that, are favourable conditions for the development of mountain waves.

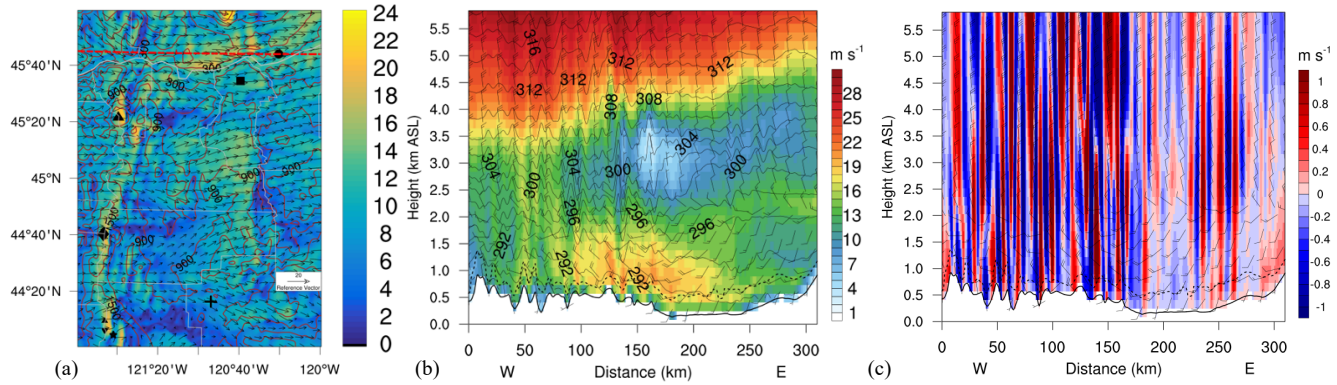

Figure 4. (a) Simulated wind field at 100 m AGL. The big triangle, diamond, cross, square and circle denote locations of Mt. Hood, Mt. Jefferson, Prineville, Wasco instrument site, and the wind farm, respectively. Sisters and Broken Top mountains located in lower left corner are shown by smaller triangles and a star, respectively. Contours show terrain elevation every 300 m. The red dashed line indicates the transect along which cross sections in (b) and (c) are taken. Note that the cross sections in (b) and (c) extend beyond the bounds of this plot. (b) Cross section of horizontal wind speed from west to east through the wind farm. Wind speeds are colour shaded, lines denote potential temperature [K], the boundary layer top is dashed. (c) Cross section of vertical wind speeds through the wind farm at 04:00 UTC on 24 September 2016.

Mountain waves are possible when the nondimensional mountain height is in the order of 1 (Mastaler and Reno 2003). Therefore, we calculated the nondimensional mountain height and the Scorer parameter (Figure 6) from the WRF simulations at Troutdale. The nondimensional mountain height was calculated using the bulk method by Reinecke and Durran (2007), using an average free stream velocity between 1,500 and 7,000 m, a mountain height of 1,500 m, and a Brunt–Väisälä frequency between 0 m and 7,000 m. Mountain waves are possible because the nondimensional mountain height was high during the entire day (Figure 6). In fact, the horizontal wind field shows waves until approximately 15:00 UTC.

The Scorer parameter (Eq. 1) is a further measure to determine whether mountain waves develop:

$$l^2 = \frac{N^2}{U^2} - \frac{1}{U}\frac{d^2U}{dz^2} \qquad (1)$$

where $U(z)$ is the speed of the basic-state flow and $N(z)$ is the Brunt-Väisälä frequency, with z being the vertical coordinate (Durran, 2003). According to Scorer (1949), waves are possible if atmospheric stability decreases or wind speed increases with height (Lindsay 1962). In our case, wind speeds increase with height (Figure 5). Moreover, when the Scorer parameter is nearly constant with height, conditions are favourable for vertically propagating mountain waves. Trapped lee waves can be expected when the Scorer parameter l decreases with height. Figure 6 (b) shows that the Scorer parameter from model output at Troutdale at 01:00 UTC increases with height up to ~200 m and is mostly constant above that. At 04:00 UTC, it also increases with height up to ~200 m, exhibits multiple maxima until about 1100 m, and is nearly constant with height above that. Multiple maxima indicate that multiple wave systems may occur simultaneously. The slight change of the profile in time indicates that the simulated mountain waves may change their propagation characteristics slightly over time.

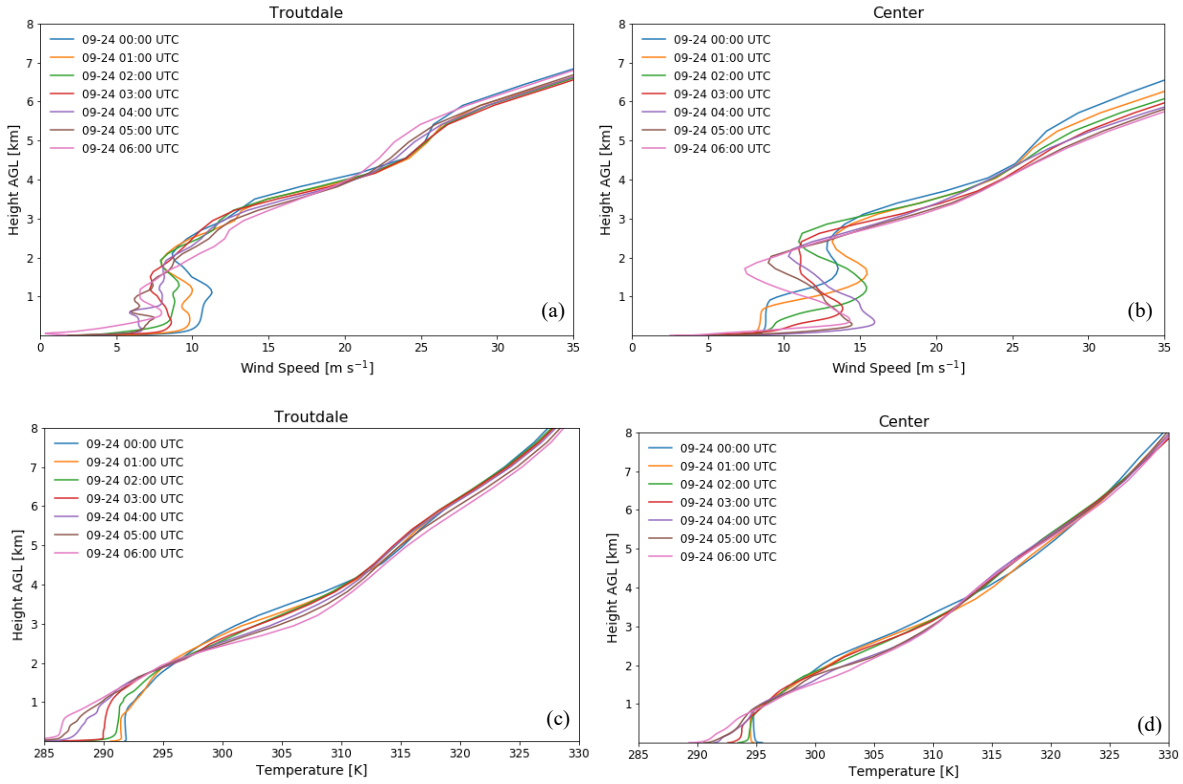

Figure 5. Simulated WRF wind speed [(a), (b)] and potential temperature profiles [(c), (d)] at Troutdale [(a), (c)] and a location in the centre of the modelling domain, east of the Cascades, [(b), (d)] during mountain wave activities.

3.2 Comparison of model simulations with observations on 24 September 2016

We will now compare the model simulations with observations to see how well the model captures mountain waves. We will look at satellite images and lidar and sodar observations at Wasco (Figure 2). Note that lidar and sodar observations represent data collected at a single point in space; therefore, signals in these data will indicate nonstationary mountain waves.

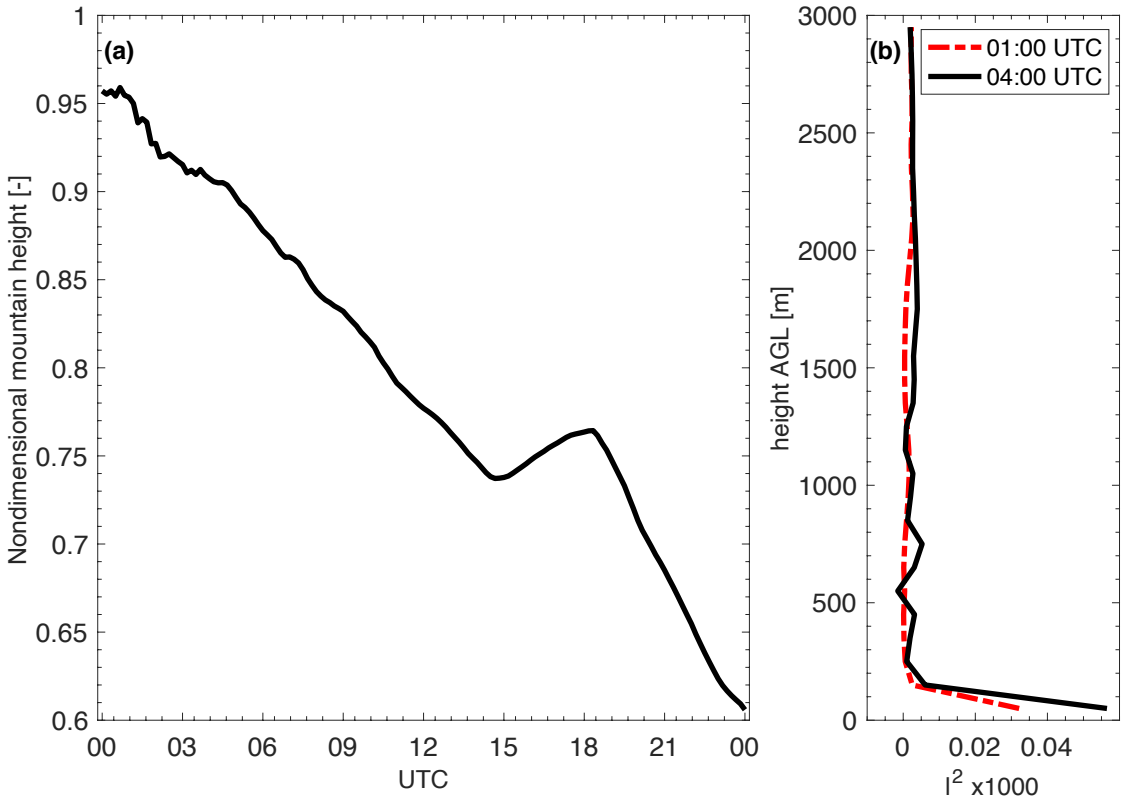

Figure 6. **(a) Nondimensional mountain height as a function of time of day (UTC), (b) Scorer parameter at 01:00 UTC (dashed red), and at 04:00 UTC (solid) from model simulations.**

3.2.1 GOES satellite imagery

GOES visible reflectances at 1000 m resolution and 630 nm wavelengths (Figure 7 (a)) show a wavy cloud pattern similar to the simulated wind field in Figure 4 (a) on 23 September 2016, from 19:30 UTC until sunset (shown for 22:00 UTC on 23 September 2016. After sunset, visible satellite images cannot reveal any signals. The appearance of mountain waves during that time matches with the model simulations in which mountain waves appeared starting on 23 September 2016, around 16:00 UTC. From the clouds, a wavelength of approximately 8 km was deduced (Figure 7 (a, b)). The wavelength is calculated by averaging the cloud reflectance from 44.4°N to 46.6°N along 121°W to 121.3°W, shown by the meridional distribution in Figure 7 (b). Note the spatial heterogeneity in the cloud field (Figure 7 (a)), which indicates similar variability in the manifestation of mountain waves.

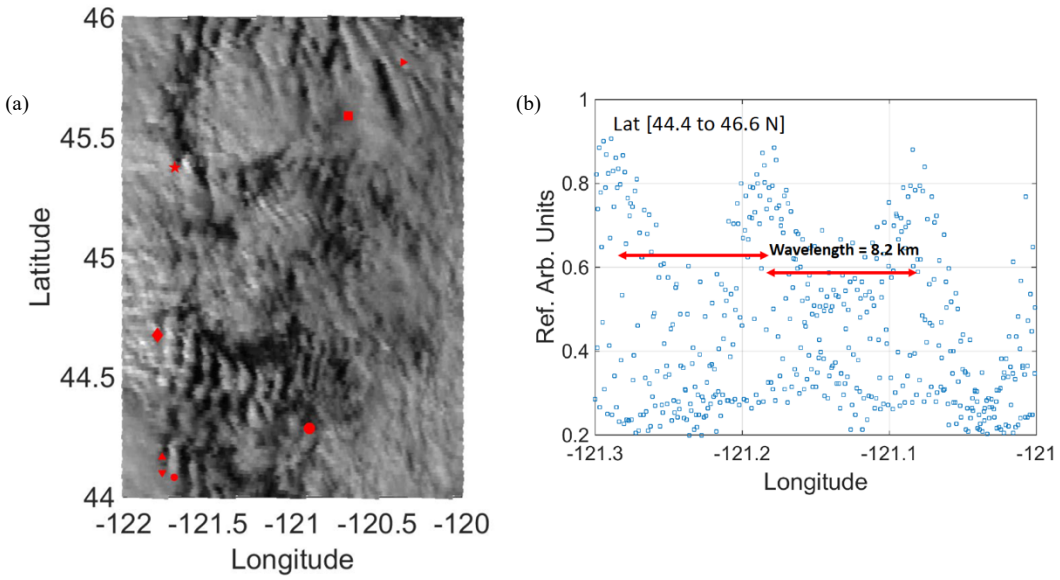

Figure 7. (a) GOES-14 satellite image on 23 September 2016, at 22:00 UTC. The red dots represent the same locations as in Figure 4. (b) The dots denote cloud reflectance in arbitrary units (counts or normalized data) covering latitude 44.4 to 46.6 N at 22:00 UTC.

3.2.2 Lidar and sodar observations

Observations at fixed locations (such as from lidar or sodar) can reveal the presence of trapped lee waves through temporal fluctuations in the lee-wave pattern (Bougeault et al. 1993, Wilczak et al. 2019). Periods of alternating high and low wind speeds were observed at Wasco from all collocated remote sensing instruments as well as in the simulated horizontal wind field (Figure 8). Good agreement is found between data from all instruments (Figure 8a–c), as waves manifest in all instruments starting near 02:00 UTC, increasing in amplitude until a maximum near 10:00 UTC, then decreasing. Clear patterns of waves are discernible in both measured and simulated wind speeds. However, during the high-wind-speed periods, WRF overpredicted the wind speed from 06:00 to 09:00 UTC. Further, the phase of the waves in WRF did not always match that of the observations. In general, the waves are well captured in time and magnitude.

3.2.3 Wavelengths and speed of wave propagation observed on 24 September 2016

From an operational forecasting perspective, knowing when mountain waves will influence wind power and for which period of time can be valuable for forecasting for power trading, and forecasting the balancing requirements in the power system – from both a regulatory and economic perspective. Nearly stationary mountain waves lend to less short-term volatility in energy production, but potentially a still large deviation from scheduled production and therefore large balancing requirements for the duration of the event. Such stationary events can lead to large and costly imbalances for power producers. Large wavelengths

(>18 km) can exacerbate the imbalance for both grid operators and power producers by reducing (or enhancing) production over multiple wind farms at once, whereas shorter wavelengths (where several wavelengths occur within one wind production region) will tend to have some areas of enhanced production and other areas of reduced production, resulting in a beneficial netting effect. Quickly propagating mountain waves produce the netting effect on a temporal scale, so that while short-term imbalances can be large and require costly balancing reserves, longer term imbalances may be small. Balancing costs at all described time scales are important to grid operators and energy producers, but they require different planning. We therefore investigate whether our model simulations are able to forecast the speed of the mountain wave propagation, as well as their wavelengths.

From the spatial pattern of mountain waves in the 100 m wind speeds, we extract wind speeds along 45.6 degrees north latitude and calculate the power spectrum using the fast Fourier transform (FFT) (Figure 9). The spatial pattern of the waves at 50 and 200 m are similar (not shown). At this latitude, most of the WFIP2 sodar sites are located. Evidently, most of the power variances are explained by low-frequency waves and large wave patterns (Figure 9b). For wavelengths shorter than 8 km the associated power variance is negligible. From the analysis in Section 3.2, we identified that mountain wave wavelengths range from 8–18 km. In that range, the bulk of the power variance occurs between 23 September 22:00 UTC, and 24 September 04:00 UTC. Therefore, we reconstruct the wind field by filtering it with respect to wavelengths between 8 km and 18 km.

To confirm our choice of wavelength range, we show Hövmöller diagrams of the original and reconstructed hub-height wind speed (Figure 10) at the targeted latitude. There is a mountain wave event particularly distinguishable between 23 September 22:00 UTC, and 24 September 04:00 UTC (Figure 10 (a) and power variance in Figure 9 (b)), which is well captured by the reconstructed wave pattern (Figure 10 (b)). To determine the wave period, Figure 10 (c) shows the power spectrum of the reconstructed (8-18 km wavelength) and observed hub-height wind speed. We have removed the low-frequency wave signals (24 h and 12 h) from both the observed and simulated time series to focus on high-frequency waves. We chose the wave periods to be between 1 h and 4 h because that is within the time range of our interest (22:00 UTC to 04:00 UTC) and it explains the majority of the power variance by the simulated mountain waves (Figure 9 (b)).

Finally, we reconstruct the simulated wind field at each time step using band-pass filtering (FFT), wavelength and wave period constraints (Xia et al. 2020), and compare that with the observations (Figure 11). Because the mountain wave event that we are interested in is particularly visible in the simulations between 22:00 UTC and 04:00 UTC the next day, we only plot that period for comparison. The reconstructed wind speed time series shows a 1-h shift compared to the observations. In addition, we can deduce a wave period of 2.5 h; with a wavelength of 8-18 km, we estimate the wave speed to be 1.5 m s^{-1}. The results seem to be sensitive to the chosen grid point and the period of interest (not shown). For instance, we performed a similar analysis using a grid point that is about 7 km (10 grid points) away from the original one. The simulated wind field looks similar to that of Figure 11 but the resemblance with the observations is weaker.

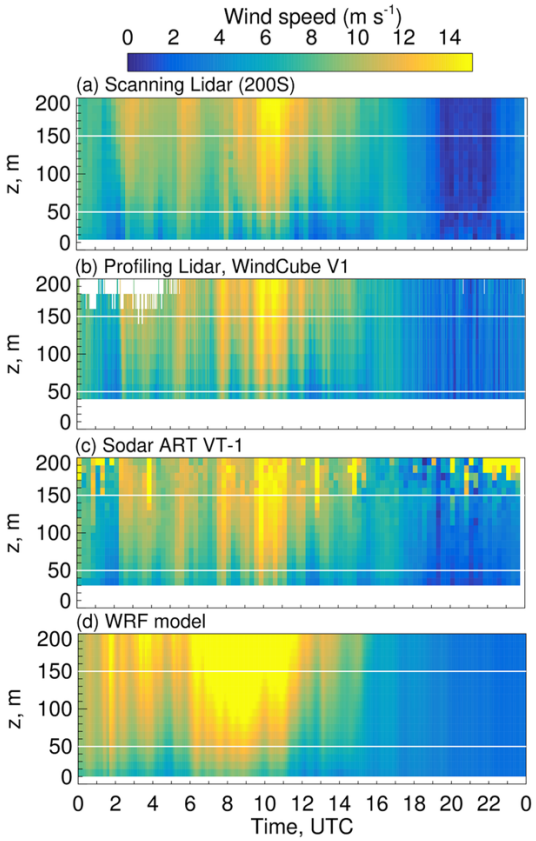

Figure 8. Observed wind speeds up to 200 m above ground as a function of time from the (a) scanning Doppler lidar (200S), (b) the profiling lidar (Wind Cube, V1), (c) the sodar (ART VT1), and (d) simulated wind speeds at Wasco on 24 September 2016. Two horizontal white lines in each panel indicate the 50–150 m layer where turbines operate.

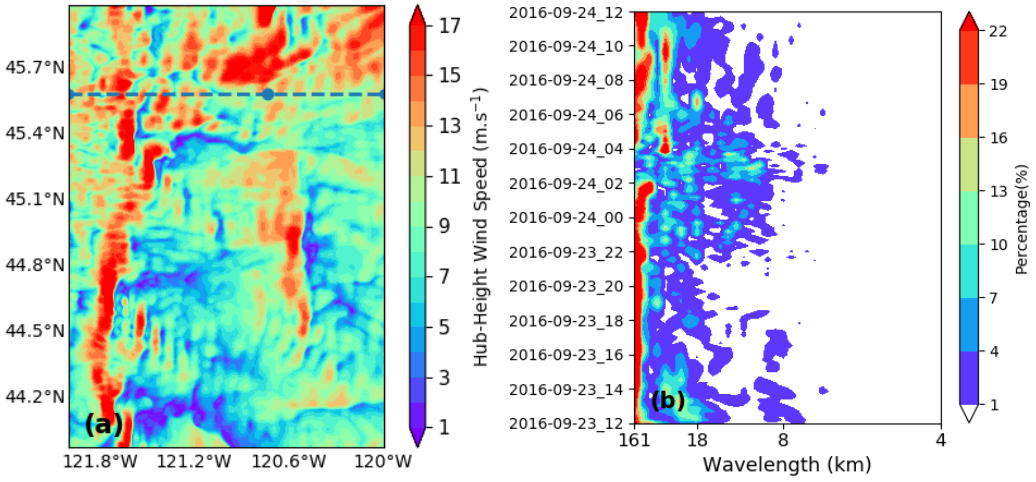

Figure 9. (a) Simulated horizontal wind speeds [m s^{-1}] at 100 m on 24 September 2016, 02:00 UTC; the dashed line at 45.6 degrees north indicates where the FFT was taken. The dotted point represents the location of the sodar site at Van Gilder Road close to Wasco. (b) Hövmöller diagram of power variance with respect to wavelength at the targeted latitude.

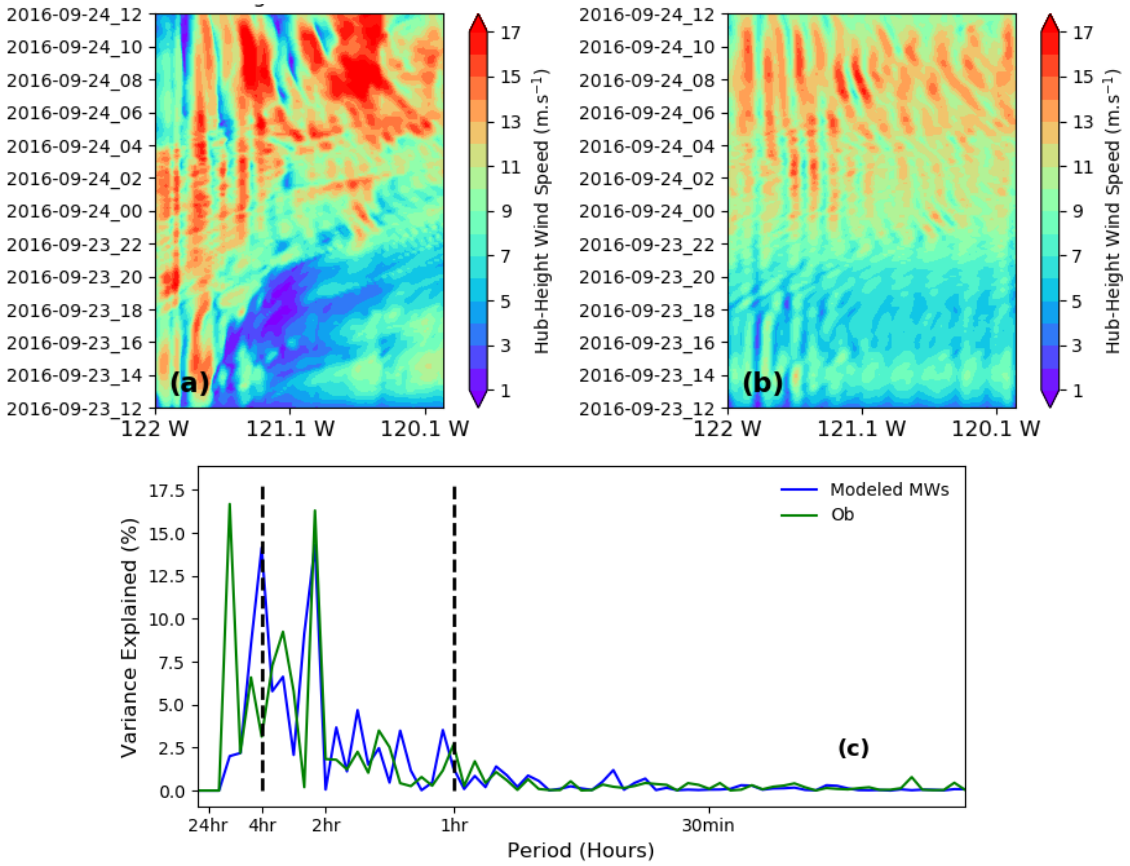

Figure 10. (a) Hövmöller diagram of simulated hub-height wind speeds at the targeted latitude; (b) Same as (a), but showing the filtered wind speeds with wavelengths from 8-18 km; (c) Observed (green) and reconstructed (blue) power spectrum on the time domain for 24 September 2016. The simulated FFT was reconstructed with wavelengths from 8-18 km. The dashed lines indicate the wave period of interest from 1-4 hours.

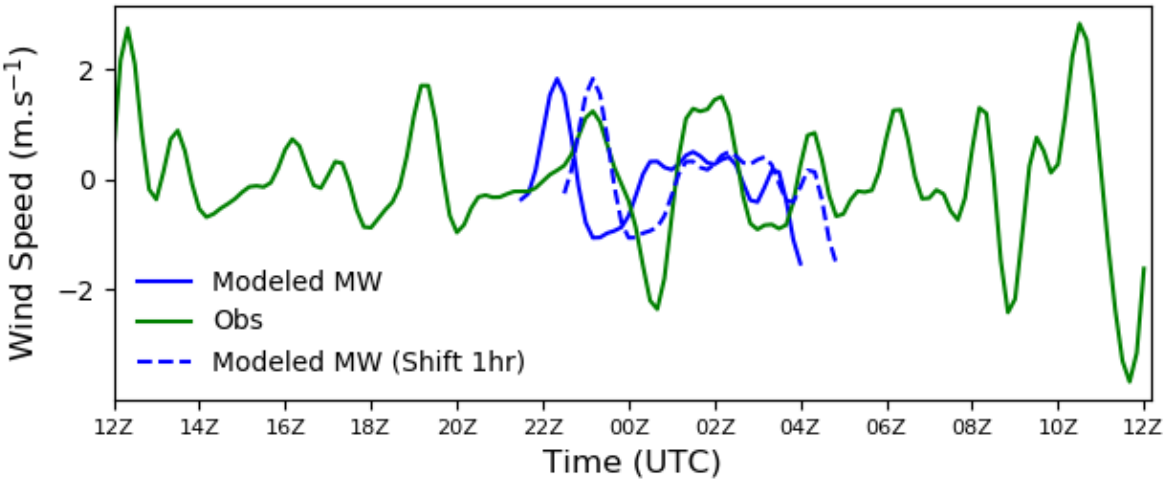

335 **Figure 11. 100 m (green) observed and (blue) reconstructed simulated wind speed time series from 23 September 2016, 12:00 UTC, until 24 September 2016, 12:00 UTC. The simulated wind speeds were reconstructed with wavelengths from 8-18 km, and periods from 1-4 h, while the observed winds were reconstructed with periods from 1-4 h. The simulated mountain waves were plotted from 22:00 UTC to 04:00 UTC because the mountain wave event that we are interested in is particularly visible at that time. The dashed time series indicates the simulated mountain waves that were shifted by 1 h.**

340

3.3 Impact of mountain waves on power output

The impact of mountain waves on wind power plant output in the Pacific Northwest has been anecdotally recognized by wind energy meteorologists for about a decade, and operational meteorologists know to expect additional power-generation volatility when mountain waves are present. The first time this impact was documented in a peer-reviewed journal was in

345 Wilczak et al. (2019). Wilczak et al. (2019) confirmed signals in wind plant power output through spectra by showing that the frequency range of dominant energy is consistent with the period of mountain waves identified via satellite and wind speed observations. In this paper, we provide additional proof of the impact of mountain waves on power output by analysing wind farm power output from another wind farm in the area on a different day. We use nacelle wind speeds and model wind speeds as well as individual turbine and total farm power output.

350 First, power output from a wind plant in the study area is compared to measured wind speeds at the turbines and WRF output. Figure 12 shows the direct influence that mountain waves can have on power output of a single turbine. The number of wave crests (approximately 6) agrees well with the lidar and sodar observations in Figure 8. During the time when mountain waves were present (00:00–12:00 UTC), the winds were fairly strong (approximately 10 m s^{-1}). Oscillations in measured wind speeds were around 5 m s^{-1} and agree well with WRF simulations in timing and magnitude. These oscillations in wind speed

355 correspond with oscillations in observed turbine power. During this particular event, these oscillations are at such a critical point (region 2) in the power curve that small oscillations about the overall mean flow can make all the difference between full rated power (approximately 2.3 MW) or 1 MW of power at any given time.

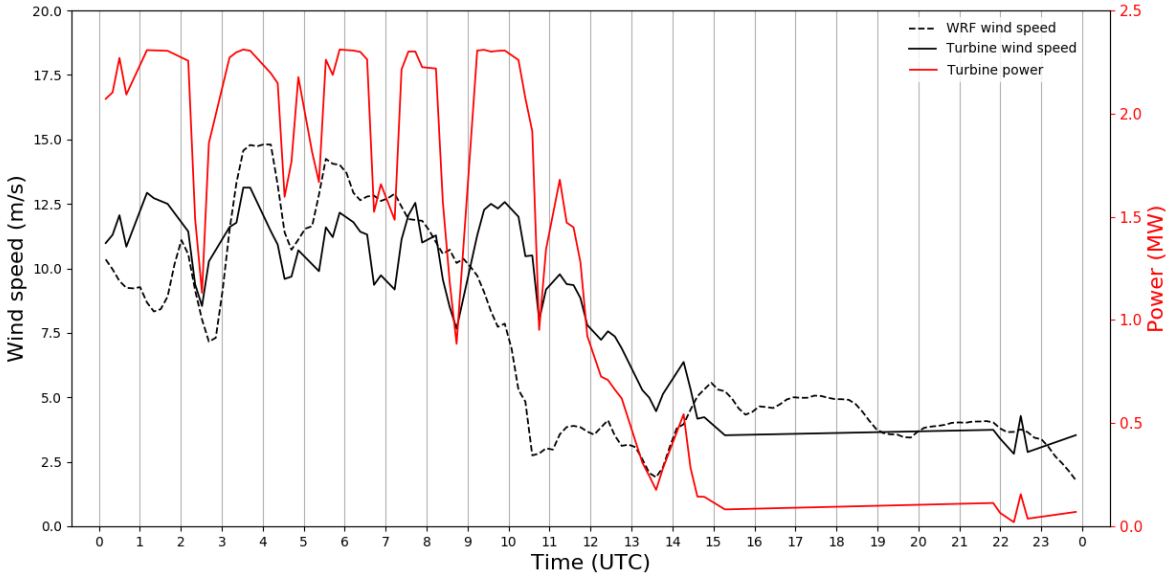

Figure 12. Time series of simulated 80 m wind speed from WRF (dashed line), observed power output from one turbine near the middle of the wind farm (red), and wind speed measurements from that turbine (black solid line).

Mountain waves can influence the total wind farm power output as well. The time series in Figure 13 shows oscillations in total power output from the entire wind farm (green), and total power output from two other wind farms in the area (orange and blue). Oscillations of approximately 25 MW exist in averaged power at the wind plant (shown in Fig. 15 as percentage) and did not get cancelled out by alternating wave influences at different locations in the wind farm. Averaged wind speeds for that wind farm indicate similar oscillations (not shown). Oscillations in power output are also visible at the other two wind farms (although those oscillations are not as regular) because mountain wake effects might play a role at those farms as well.

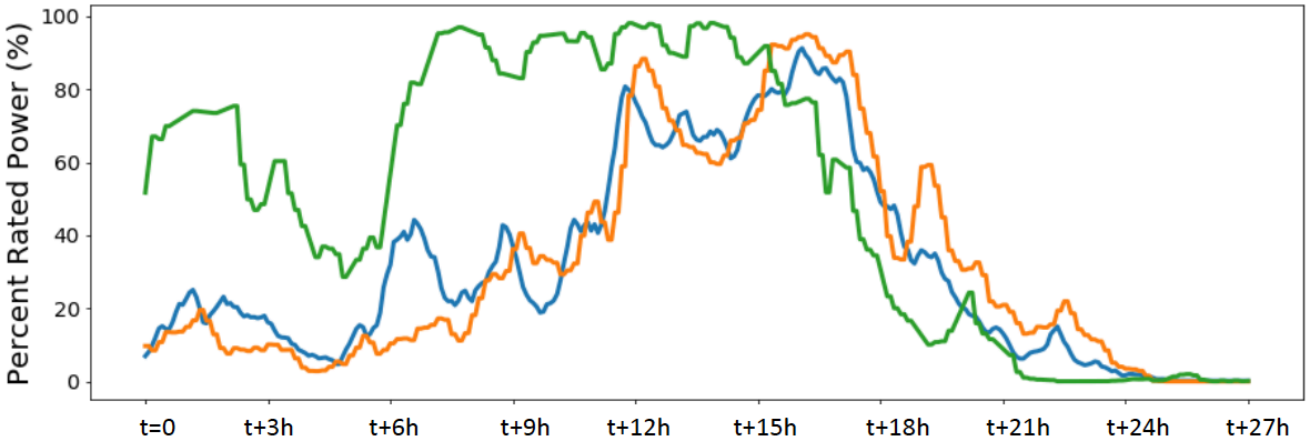

Figure 13. Time series of total power output of the wind farm used in this study (green), and two other wind farms in the area (orange and blue). The values on the x-axis show time at 3 h intervals.

4 Discussion

The previous sections discussed a mountain wave event in the Columbia Basin through simulations and observations. The signature of these waves was apparent in nacelle wind speeds and power observations of a wind farm in the area. In this section, we relate our findings to practical aspects in forecasting and operations.

During the event of 24 September 2016, oscillations in power caused by mountain waves are at such a critical point in the power curve (region 2, or the "steep part") that small oscillations about the overall mean flow can make all the difference between full rated power or approximately 1 MW of power at any given time. In this particular case, the few meters-per-second oscillations caused by the mountain waves have dramatic effects on power production. Even after aggregating the power output from all turbines, the power still fluctuates approximately 25 MW from mountain waves at the wind farm. For this wind plant, this is equivalent to production from approximately 10 turbines being added or lost during the presence of the wave's crests and troughs (assuming all turbines are on), given that one turbine could produce approximately 2.3 MW. About 11% of the total wind farm output is being influenced by the presence of mountain waves, which is considered significant according to the empirical threshold used in the industry that more than 10% in fluctuations (or 20 MW) is significant.

Discerning signals from mountain waves from signals caused by other phenomena in the atmosphere can be challenging. For example, mountain waves and wakes often occur concurrently, and the signals in time series of wind speed when analysing observations at a single site, or wind turbines, can be difficult to distinguish. Mountain wakes impacting wind turbines in the Columbia Basin are mostly created by Mt. Hood. To the north of a Mt.-Hood wake are the Gorge gap-flow westerlies and to the south are geostrophic southwesterlies that can sometimes mix down to the southernmost and highest-elevation turbines in the area. The instability of the mountain wake edge leads to much volatility and it is common for entire wind power plants to go back and forth between being in the lull and being at full power. Concurrently occurring mountain wakes and waves can

lead to high-volatility periods where forecasts range from zero to full power. Power data might also include various aspects, such as curtailments and turbine wakes. During our case study, the wind farm was not curtailed. Additionally, analyses of the simulated spatial wind field, as well as cloud cover by GOES satellite data (not shown), indicate that the mountain waves appeared to shift around without systematic upstream or downstream propagation on 24 September 2016. This points to nonlinear interactions between different waves, and that the dominant dynamics are nonlinear (Nance and Durran 1997, Nance and Durran 1998, Part II). Nonetheless, mountain waves showed up in periodic signals in wind speed and power (Figs. 9–12). We analysed the wavelengths of the mountain waves; they ranged from 8–10 km in the two case studies (24 September 2016, and 11 November 2016 (Wilczak et al. 2019)) and were well captured by the numerical simulations. Future studies will include further quantification of wavelengths and whether both shorter and longer wavelengths appear simultaneously in a wind-farm region. During periods with shorter wavelengths, only parts of a wind plant will experience low wind speeds, while other parts will be exposed to stronger winds, which can result in cancelling effects so that power output is minimally affected. During these cases, accurate mountain wave and wavelength forecasts are important for wind plant operators to save on balancing costs. On the contrary, if wavelengths are long, entire regions can oscillate between near-full and near-zero power and, in particular situations, a lull over an entire region can occur, encompassing multiple wind farms. Similarly, problems arise if wind farms are spaced apart such that two wind plants happen to be in lulls while high wind speeds occur between them. Knowing when to trust model-wavelength forecasts will be the subject of future studies. In terms of speed of wave propagation, our research has shown that not all mountain waves exhibit the same speed. In the case of 24 September 2016, the simulated waves move with a speed of approximately 1.5 m s^{-1} (section 3.2.3); in the case of 11 November 2016 (Wilczak et al. 2019), the simulated waves move with 2 m s^{-1} (computed the same way as in section 3.2.3). This seems to contradict our findings from analysing GOES satellite data which showed no systematic propagation. Both extended wavelength and wave speed analyses are the subjects of future work.

From an operational perspective, using high-resolution forecasts that can resolve mountain waves are crucial to predict power output at a particular wind farm. The grid spacing of the simulations should be fine enough for a forecaster to recognize mountain waves. For example, even though waves are reflected in a wind field simulated on a 3 km grid, they might not be recognized as such because the waves are too wide or missing clear distinctions between high and low wind speeds that are the result of wave crests and troughs. Sharp gradients between near-zero and near-full power need to be recognizable when a forecaster looks at model simulations. Even though it is impossible to nail down the exact location of the wave crests and troughs, speed of propagation, magnitudes of wind speeds, or wavelength, the forecaster can recognize the risk for mountain waves and associated large drops or surges in power. Additionally, if high-resolution forecasts are misinterpreted (i.e., the position of wave crests and troughs are overly trusted), they have the potential to degrade a forecast. For a forecaster, it is key to be informed about the occurrence of mountain waves in order to act (e.g., assign more balancing reserves for volatility to make sure a wide range of possible production is covered). At forecasts near full power, a mountain wave event can be indicative of reductions of power. In any event, mountain wave forecasts should not be used as deterministic solutions.

5 Summary and Conclusions

We have shown that mountain waves can occur frequently in areas of complex terrain and can be modelled with mesoscale models as was confirmed by observations. Mountain waves can impact wind turbine and wind farm power output and, therefore, should be considered in complex terrain when designing, building, and forecasting for wind farms. Mountain waves impact the quantity of the wind resource and the quality by impacting temporal and spatial variability.

We suggest that forecasters be informed when mountain waves occur and, therefore, to be informed about wind variability to act accordingly (e.g., when setting day-ahead positions for balancing reserves and schedules). Even though the nuances of wavelength, wave propagation, or exact location are not easy to identify or simulate (because they depend on the upstream wind speed and direction as well as the vertical stability profile), being aware when mountain waves are forecast is key in operational wind energy forecasting in complex terrain. Information about the occurrence of mountain waves adds value by communicating the risk and probability of variability in power output, which helps planning for possible extreme situations. Depending on the mountain wave event and the size and shape of wind plants, effects tend to cancel out over large areas. For this to be true, wind farms should be laid out such that the windward and leeward portions are equally exposed to the mountain wave pattern. Determining the best size and orientation of wind plants to minimize mountain wave effects would be a recommendation for future studies.

Future studies should also include analyses of aggregates over larger regions to see wave patterns through wind plants as well as interactions with mountain wakes. Often, particular regions have their own peculiarities, which might also be a function of turbine age and kind, location, or elevation.

Code/Data availability

The measurement data that support the findings of this study are openly available in Data Archive and Portal (DAP), https://a2e.energy.gov/data. The DAP establishes a sustained data management structure with protocols and access to assure massive datasets resulting from DOE A2e (Atmosphere to Electrons) efforts will have the quality needed for scientific discovery and portals required to make data available to a broad stakeholder group. The WRF simulations and code are available from the lead author upon request. Data from wind farms are proprietary and were used under license for this study, and are therefore not publicly available.

Author contributions

Caroline Draxl – prepared the manuscript with contributions from all co-authors; conceptualization, formal analysis, investigation, project administration, resources, software, supervision, validation, visualization, writing (original draft, review and editing)

Rochelle Worsnop – conceptualization, formal analysis, data curation, investigation, resources, software, validation, visualization, writing (original draft, review and editing)

Geng Xia – formal analysis, data curation, investigation, resources, software, validation, visualization, writing (original draft)

Yelena Pichugina – formal analysis, data curation, investigation, resources, software, validation, visualization, writing (original draft)

Duli Chand – formal analysis, data curation, investigation, resources, software, visualization, writing (original draft)

Julie Lundquist – conceptualization, formal analysis, writing (original draft, review, editing)

Justin Sharp – conceptualization, writing (original draft)

Garrett Wedam – conceptualization, writing (original draft)

James Wilczak – conceptualization, formal analysis, writing (original draft, review, editing)

Larry Berg – conceptualization

The authors declare that they have no conflict of interest.

Acknowledgements

The authors thank the WFIP2-experiment participants who aided in the deployment and the collection of remote sensing data and our colleagues who monitored, quality controlled and provided data to the data archive portal (DAP). A special thanks go to Joe Cline (DOE), Melinda Marquis (NOAA), and Jim McCaa (Vaisala) for their effort to propose, design, and lead the WFIP2. The research was performed using computational resources sponsored by the Department of Energy's Office of Energy Efficiency and Renewable Energy and located at the National Renewable Energy Laboratory. Lastly, we thank two anonymous reviewers for their comments, which helped improve the manuscript.

This work was authored in part by the National Renewable Energy Laboratory, operated by Alliance for Sustainable Energy, LLC, for the U.S. Department of Energy (DOE) under Contract No. DE-AC36-08GO28308. Funding was provided by the U.S. Department of Energy Office of Energy Efficiency and Renewable Energy Wind Energy Technologies Office. This work was partially supported by the National Oceanic and Atmospheric Administration (NOAA) Atmospheric Science for Renewable Energy (ASRE) program. The views expressed in the article do not necessarily represent the views of the DOE or the U.S. Government. The U.S. Government retains and the publisher, by accepting the article for publication, acknowledges that the U.S. Government retains a nonexclusive, paid-up, irrevocable, worldwide license to publish or reproduce the published

form of this work, or allow others to do so, for U.S. Government purposes. A portion of the research was performed using computational resources sponsored by the Department of Energy's Office of Energy Efficiency and Renewable Energy and located at the National Renewable Energy Laboratory.

Appendix

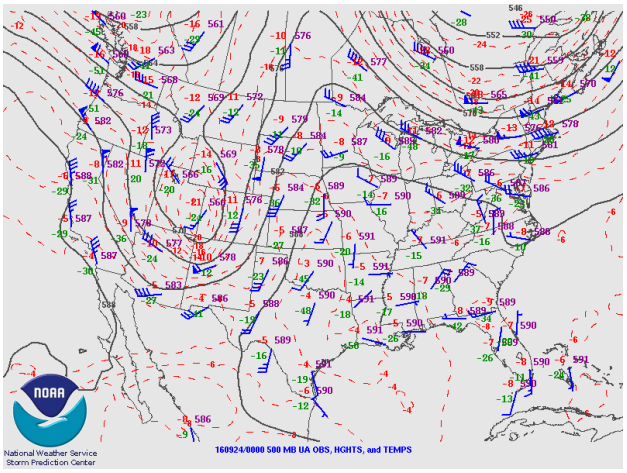

Figure 14. 500 hPa pressure (black lines), temperature (dashed red), wind barbs (blue), temperature (red numbers), and dew point (green numbers). *Source: National Weather Service*

References

Aitken, M.L., Rhodes, M.E., and Lundquist J.K.: Performance of a Wind-Profiling Lidar in the Region of Wind Turbine Rotor Disks. J. Atmos. Oceanic Technol., 29, 347–355, https://doi.org/10.1175/JTECH-D-11-00033.1, 2012.

Atmosphere to Electrons (A2e) (a). 2017. wfip2/sodar.z08.b0. Maintained by A2e Data Archive and Portal for U.S. Department of Energy, Office of Energy Efficiency and Renewable Energy. https://doi.org/10.21947/1349278. Accessed: 19 Aug. 2020.

Atmosphere to Electrons (A2e) (b). 2017. wfip2/sodar.z06.b0. Maintained by A2e Data Archive and Portal for U.S. Department of Energy, Office of Energy Efficiency and Renewable Energy. DOI: 10.21947/1409334. Accessed: 19 Aug. 2020.

Banta, R.M., Pichugina, Y.L., Brewer W.A., Choukulkar, A., Lantz, K.O., Olson, J.B., Kenyon, J., Fernando, H.J., Krishnamurthy, R., Stoelinga, M.J., Sharp, J., Darby, L.S., Turner, D.D., Baidar, S. and Sandberg, S.P.: Characterizing NWP Model Errors Using Doppler-Lidar Measurements of Recurrent Regional Diurnal Flows: Marine-Air Intrusions into the Columbia River Basin. Mon. Wea. Rev., 148, 929–953, https://doi.org/10.1175/MWR-D-19-0188.1, 2020.

Bianco, L., Djalalova, I.V., Wilczak, J.M., Olson, J.B., et al.: Impact of model improvements on 80 m wind speeds during the second Wind Forecast Improvement Project (WFIP2). Geosci. Model. Dev., 12, 4803-4821; https://doi.org/10.5194/gmd-12-4803-2019, 2019.

Bodini, N., Lundquist, J. K., Krishnamurthy, R., Pekour, M., Berg, L. K., and Choukulkar, A.: Spatial and temporal variability of turbulence dissipation rate in complex terrain, Atmos. Chem. Phys., 19, 4367-4382, https://doi.org/10.5194/acp-19-4367-2019, 2019.

Dee, D.P., Uppala, S.M., Simmons, A.J., Berrisford, P., Poli, P., Kobayashi, S., Andrae, U., Balmaseda, M.A., Balsamo, G., Bauer, P., Bechtold, P., Beljaars, A.C.M., van de Berg, L., Bidlot, J., Bormann, N., Delsol, C., Dragani, R., Fuentes, M., Geer, A.J., Haimberger, L., Healy, S.B., Hersbach, H., Hólm, E.V., Isaksen, L., Kållberg, P., Köhler, M., Matricardi, M., McNally, A.P., Monge-Sanz, B.M., Morcrette, J.-J., Park, B.-K., Peubey, C., de Rosnay, P., Tavolato, C., Thépaut, J.-N. and Vitart, F.: The ERA-Interim reanalysis: configuration and performance of the data assimilation system. Q.J.R. Meteorol. Soc., 137: 553-597. https://doi.org/10.1002/qj.828, 2011.

Doyle, J. D., and Durran, D. R.: The Dynamics of Mountain-Wave-Induced Rotors. J. Atmos. Sci., 59, 186–201, https://doi.org/10.1175/1520-0469(2002)059<0186:TDOMWI>2.0.CO;2, 2002.

Durran, D. R.: Lee waves and mountain waves. https://doi.org/10.1016/B0-12-227090-8/00202-5, 2003.

Durran, D. R.: Mountain Meteorology. Lee Waves and Mountain Waves, Encyclopedia of Atmospheric Sciences (Second Edition). Academic Press, pp 95-102, ISBN 9780123822253, https://doi.org/10.1016/B978-0-12-382225-3.00202-4, 2015.

Fritts, D. C.: Gravity Waves Overview, Encyclopedia of Atmospheric Sciences (Second Edition), Academic Press, pp 141-152, ISBN 9780123822253, https://doi.org/10.1016/B978-0-12-382225-3.00234-6, 2015.

Grubišić, V., and Billings, B. J.: The Intense Lee-Wave Rotor Event of Sierra Rotors IOP 8. J. Atmos. Sci., 64, 4178–4201, https://doi.org/10.1175/2006JAS2008.1, 2007.

Haupt, S.E., Kotamarthi, R., Feng, Y., Mirocha, J.D., Koo, E., Linn, R., Kosovic, B., Brown, B., Anderson, A., Churchfield, M.J., Draxl, C., Quon, E., Shaw W., Berg, L., Rai, R., Ennis, B.L: Second year report of the atmosphere to electrons mesoscale to microscale coupling project: nonstationary modelling techniques and assessment. Pacific Northwest National Laboratory, Richland, WA, Technical Report PNNL-26267, 2017.

Klemp, J. B., and Lilly, D. K.: Numerical Simulation of Hydrostatic Mountain Waves. J. Atmos. Sci., 35, 78–107, https://doi.org/10.1175/1520-0469(1978)035<0078:NSOHMW>2.0.CO;2, 1978.

Lindsay, C. V.: Mountain Waves in the Appalachians. Mon. Wea. Rev., 90, 271–276, https://doi.org/10.1175/1520-0493(1962)090<0271:MWITA>2.0.CO;2, 1962.

Mahalov, A., Moustaoui, M., and Grubišić, V.: A numerical study of mountain waves in the upper troposphere and lower stratosphere. Atmos. Chem. Phys., 11, 5123-5139, https://doi.org/10.5194/acp-11-5123-2011, 2011.

Miglietta, M. M., Zecchetto, S., and De Biasio, F.: A comparison of WRF model simulations with SAR wind data in two case studies of orographic lee waves over the Eastern Mediterranean Sea, Atmospheric Research, Volumes 120–121, pp 127-146, ISSN 0169-8095, https://doi.org/10.1016/j.atmosres.2012.08.009, 2013.

Nakanishi, M., Niino, H.:Development of an improved turbulence closure model for the atmospheric boundary layer. J Meteorol Soc of Japan Ser II, 87(5):895–912, DOI 10.2151/jmsj.87.895, 2009.

Nappo, C. J.: Mountain Waves, International Geophysics, Academic Press, Volume 102, pp 57-85, ISSN 0074-6142, ISBN 9780123852236, https://doi.org/10.1016/B978-0-12-385223-6.00003-3, 2012.

Olson, J., Kenyon, J. Djalalova, I. Bianco, L., Turner, D., Pichugina, Y., Choukulkar, A., Toy, M., Brown, J. M., Angevine, W., Akish, E., Bao, J.-W., Jimenez, P., Kosovic, B., Lundquist, K., Draxl, C., Lundquist, J. K., McCaa, J., McCaffrey, K.,

Lantz, K., Long, C., Wilczak, J., Banta, R., Marquis, M., Redfern, S., Berg, L. K., Shaw, W., and Cline, J. 2019. Improving Wind Energy Forecasting through Numerical Weather Prediction Model Development. Accepted by: Bull. Amer. Meteor. Soc.

Pichugina, Y. L., Banta, R. M., Bonin, T., Brewer, W. A., Choukulkar, A., McCarty, B. J., Baidar, S., Draxl, C., Fernando, H. J., Kenyon, J., Krishnamurthy, R., Marquis, M., Olson, J., Sharp, J., and Stoelinga, M.: Spatial Variability of Winds and HRRR–NCEP Model Error Statistics at Three Doppler-Lidar Sites in the Wind-Energy Generation Region of the Columbia River Basin. J. Appl. Meteor. Climatol., 58, 1633–1656, https://doi.org/10.1175/JAMC-D-18-0244.1, 2019.

Pichugina, Y.L., Banta, R.M., Bonin, T., Brewer, W.A., Choukulkar, A., McCarty, B.J., Baidar, S., Draxl, C., Fernando, H.J., Kenyon, J., Krishnamurthy, R., Marquis, M., Olson, J., Sharp, J., and Stoelinga, M.: Spatial Variability of Winds and HRRR–NCEP Model Error Statistics at Three Doppler-Lidar Sites in the Wind-Energy Generation Region of the Columbia River Basin. J. Appl. Meteor. Climatol., 58, 1633–1656, https://doi.org/10.1175/JAMC-D-18-0244.1, 2019.

Pichugina, Y., Banta, R., Brewer, W.A., Bianco, L., Draxl, C., Kenyon, J., Lundquist, J.K., Olson, J., Turner, D.D., Wharton, S., Wilczak, J., Baidar, S., Berg, L., Fernando, H.J.S., McCarty, B., Rai, R., Roberts, B., Sharp, J., Shaw, W., Stoelinga, M. and Worsnop, R.: Evaluating the WFIP2 updates to the HRRR model using scanning Doppler lidar measurements in the complex terrain of the Columbia River Basin, JRSE, submitted, 2020.

Rasheed, A., Süld, J. K., and Kvamsdal, T.: A Multiscale Wind and Power Forecast System for Wind Farms, Energy Procedia, Volume 53, pp 290-299, ISSN 1876-6102, https://doi.org/10.1016/j.egypro.2014.07.238, 2014.

Reichmann, H.: Cross-Country Soaring (Streckensegelflug), Thomson Publications, 150 pp., ISBN-13: 978-1883813017, 1978,

Rhodes, M.E., Lundquist, J.K.: The Effect of Wind-Turbine Wakes on Summertime US Midwest Atmospheric Wind Profiles as Observed with Ground-Based Doppler Lidar. Boundary-Layer Meteorol 149, 85–103. https://doi.org/10.1007/s10546-013-9834-x, 2013.

Scorer, R. S.: Theory of waves in the lee of mountains. Q. J. R. Meteorol. Soc., 75: 41-56. https://doi.org/10.1002/qj.49707532308, 1949.

Shaw, W. J., Berg, L. K., Cline, J., Draxl, C., Djalalova, I., Grimit, E. P., Lundquist, J. K., Marquis, M., McCaa, J., Olson, J. B., Sivaraman, C., Sharp, J., and Wilczak, J. M.: The Second Wind Forecast Improvement Project (WFIP 2): General Overview. Bull. Amer. Meteor. Soc., 100, 1687–1699, https://doi.org/10.1175/BAMS-D-18-0036.1, 2019.

Skamarock, W. C., Klemp, J. B., Dudhia, J., Gill, D. O., Barker, D., Duda, M. G., Huang, X. Y., Wang, W., Powers, J. G.: A Description of the Advanced Research WRF Version 3 (No. NCAR/TN-475+STR). University Corporation for Atmospheric Research. https://doi.org/10.5065/D68S4MVH, 2008.

Smith, R., Doyle, J. D., Jiang, Q., and Smith, S.: Alpine gravity waves: Lessons from MAP regarding mountain wave generation and breaking. Q. J. R. Meteorol. Soc.133: 917 – 936, https://doi.org/10.1002/qj.103, 2007.

Smith, S. A.: Observations and simulations of the 8 November 1999 MAP mountain wave case. Q. J. R. Meteorol. Soc. (2004), 130, pp. 1305–1325, https://doi.org/10.1256/qj.03.112, 2003.

Smith, S. A., and Broad, A. S.: Horizontal and temporal variability of mountain waves over Mont Blanc. Q. J. R. Meteorol. Soc. 129, pp. 2195–2216, https://doi.org/10.1256/qj.02.148, 2003.

U. S. Department of Energy: Wind Vision: A New Era for wind power in the United States. http://www.energy.gov/sites/prod/files/WindVision_Report_final.pdf. Last accessed: March 17, 2020.

Vosper, S. B., Wells, H., Sinclair, J. A., and Sheridan, P. F.: A climatology of lee waves over the UK derived from model forecasts. Royal Met Soc, 20,4, pp 466-481, https://doi.org/10.1002/met.1311, 2012.

Wells, H., Vosper, S.B., Webster, S., Ross, A.N., and Brown, A.R.: The impact of mountain wakes on the drag exerted on downstream mountains. Quart. J. Roy. Meteor. Soc., 134, 774 677–687. https://doi.org/10.1002/qj.242, 2008.

Wilczak, J. M., Stoelinga, M., Berg, L. K., Sharp, J., Draxl, C., McCaffrey, K., Banta, R. M., Bianco, L., Djalalova, I., Lundquist, J. K., Muradyan, P., Choukulkar, A., Leo, L., Bonin, T., Pichugina, Y., Eckman, R., Long, C. N., Lantz, K., Worsnop, R. P., Bickford, J., Bodini, N., Chand, D., Clifton, A., Cline, J., Cook, D. R., Fernando, H. J., Friedrich, K., Krishnamurthy, R., Marquis, M., McCaa, J., Olson, J. B., Otarola-Bustos, S., Scott, G., Shaw, W. J., Wharton, S., and White, A. B.: The Second Wind Forecast Improvement Project (WFIP 2): Observational Field Campaign. Bull. Amer. Meteor. Soc., 100, 1701–1723, https://doi.org/10.1175/BAMS-D-18-0035.1, 2019.

Xia, G., Draxl, C., Raghavendra, A., Lundquist, J.K.: Validating simulated mountain wave impacts on hub-height wind speed using SoDAR observations. Submitted to Renewable Energy, 2020.